



City Research Online

## City, University of London Institutional Repository

---

**Citation:** White, M. (2021). Cycle and turbine optimisation for an ORC operating with two-phase expansion. *Applied Thermal Engineering*, 192, 116852. doi: 10.1016/j.applthermaleng.2021.116852

This is the accepted version of the paper.

This version of the publication may differ from the final published version.

---

**Permanent repository link:** <https://openaccess.city.ac.uk/id/eprint/25857/>

**Link to published version:** <https://doi.org/10.1016/j.applthermaleng.2021.116852>

**Copyright:** City Research Online aims to make research outputs of City, University of London available to a wider audience. Copyright and Moral Rights remain with the author(s) and/or copyright holders. URLs from City Research Online may be freely distributed and linked to.

**Reuse:** Copies of full items can be used for personal research or study, educational, or not-for-profit purposes without prior permission or charge. Provided that the authors, title and full bibliographic details are credited, a hyperlink and/or URL is given for the original metadata page and the content is not changed in any way.

---

---

---

City Research Online:

<http://openaccess.city.ac.uk/>

[publications@city.ac.uk](mailto:publications@city.ac.uk)

---

# Cycle and turbine optimisation for an ORC operating with two-phase expansion

Martin T. White\*

*Thermo-Fluids Research Centre, School of Mathematics, Computer Science and Engineering,  
City, University of London, Northampton Square, London, EC1V 0HB.*

---

## Abstract

Previous investigations suggest the power output from waste-heat recovery organic Rankine cycle (ORC) systems could be enhanced by up to 30% by operating with two-phase expansion, which could reduce cost and aid in the more widespread deployment of ORC technology. However, there are limited expander technologies suitable for such operation. The aim of this research is to investigate a novel ORC system that operates with wet-to-dry expansion permitting the use of a radial-inflow turbine. Specifically, through the exploitation of molecularly complex fluids the wet-to-dry expansion could be achieved across a single turbine stage, whilst the two-phase region is confined to the stator vane. Thermodynamic system optimisation is completed for potential fluids in which the degree of reaction is used to differentiate between the stator and rotor expansion processes. The results reveal that siloxanes are optimal fluids, and that for heat-source temperatures of 150, 200 and 250 °C the two-phase systems could generate up to 28%, 14% and 3% more power than single-phase systems, respectively. Following this, existing mean-line turbine methods are extended to two-phase turbines under the assumption of a two-phase homogeneous fluid under thermal equilibrium, which is supported with numerical simulations of a two-phase stator vane. The mean-line turbine optimisation for the 200 °C heat source is then conducted, with the optimal system corresponding to a turbine inlet vapour quality of 0.1 and degree of reaction of 0.4, with lower reaction leading to lower turbine efficiencies. More generally, feasible rotor geometries can be obtained, and conditions with the rotor are expected to remain subsonic. Whilst stator outlet Mach numbers range between 1.5 and 2.1, and stator throat widths below 1 mm are required, the CFD simulations indicate that wet-to-dry expansion can be successfully realised within the stator. In summary, these results provide the first positive demonstration that a 30% improvement in power output could be achieved with a two-phase ORC system operating with molecularly complex working fluids and a radial-inflow turbine.

*Keywords:* two-phase expansion; organic Rankine cycle; radial turbine; waste-heat recovery; design optimisation

---

## 1. Introduction

Globally, it is estimated that 52% of primary energy consumed is eventually lost as waste heat in the form of exhausts or effluents, of which 79% (54 PWh) of that is below 300 °C [1]. Similarly, it is estimated that within EU industry 70% (463 TWh) of waste heat is available at temperatures below that value [2]. Thus, organic Rankine cycles (ORC), which are suitable for power generation from low-temperature heat between approximately 80 and

---

\*Corresponding author

*Email address:* martin.white@city.ac.uk (Martin T. White)

400 °C, are promising candidates for waste-heat recovery power generation units. However, despite advances in recent years in the uptake of such systems, challenges surrounding high investment costs and poor thermal performance remain. Thus, continued research efforts to further improve both performance and cost of these systems are justified. Alongside the identification of innovations in system and component design, there is also a significant interest in novel thermal cycles, which includes ORC systems in which the expansion process occurs under two-phase conditions. The operating principle of an ORC system operating with two-phase expansion is identical to a standard ORC, and the system is constructed from a pump, evaporator, expander and condenser. The only difference is that the working fluid is admitted to the expander as a mixture of liquid and vapour, rather than as superheated vapour.

It is easy to justify the motivation behind two-phase expansion. For an open heat source, defined in terms of a temperature  $T_{hi}$ , mass-flow rate  $\dot{m}_h$  and constant specific heat capacity  $c_{p,h}$ , and a heat sink, defined in terms of a temperature  $T_{ci}$ , mass-flow rate  $\dot{m}_c$  and constant specific heat capacity  $c_{p,c}$ , it is readily shown that the maximum power that can be produced for a given heat-source outlet temperature is given by:

$$\frac{\dot{W}}{(\dot{m}c_p)_h} = (T_{hi} - T_{ho}) - \tau T_{ci} \left( \left( \frac{T_{hi}}{T_{ho}} \right)^{\frac{1}{\tau}} - 1 \right), \quad (1)$$

where  $T_{ho}$  is the heat-source outlet temperature and  $\tau$  is ratio of the heat capacity rates (*i.e.*,  $(\dot{m}c_p)_c/(\dot{m}c_p)_h$ ). Thus, if  $\tau \rightarrow \infty$ , Eq. 1 is at a maximum when  $T_{ho} = T_{ci}$ . For more feasible values of  $\tau$  the optimal value for  $T_{ho}$  increases, but remains close to  $T_{ci}$ . Thus, to maximise the power generation from an open heat source, it is advantageous for the power cycle to absorb as much heat from the heat source as possible. However, in conventional ORC systems, in which expansion takes place in the dry-vapour region, the ability to reduce the heat-source temperature may be restricted by the pinch-point at the beginning of evaporation, whilst the heat-transfer process between the heat source and the evaporating working fluid is associated with a relatively large exergy loss owing to the isothermal evaporation process (Fig. 1; left). By comparison, if two-phase expansion can be utilised, not only could lower heat-source outlet temperatures be realised, but the exergy destruction in the heat-addition process could be reduced by fully, or partially, removing the evaporation process (Fig. 1; right), leading to a higher power output. It is worth noting that in an ORC operating with two-phase expansion the specific enthalpy change across the expander, and the cycle thermal efficiency, will be reduced compared to single-phase systems. However, the reduction in the change in enthalpy during the heat-addition process, and the ability of two-phase systems to extract more heat from the heat source, lead to an increase in working-fluid mass-flow rate. Thus, when the product of mass-flow rate and the specific enthalpy change across the expander is considered, two-phase cycles lead to a larger power output, for which an increase of 30% is targeted within this research.

The potential of two-phase expansion, and of the trilateral flash cycle (TFC) where the expansion begins from a saturated liquid, has been discussed previously and a few notable studies are discussed here. Smith [3] studied TFC systems for recovering heat below 200 °C and found that net power outputs could be between 10% and 80% greater than a simple Rankine cycle. Fischer [4] compared the TFC to ORC systems for five different case studies, and found that for heat-source temperatures between 350 and 220 °C, the TFC could produce between 14% and 20% more power, which increases to 30% for a heat-source temperature of 150 °C. Later, Lai and Fischer [5] discussed how, depending on the fluid, the conditions at the expander outlet could be either be two-phase, or in the form of a

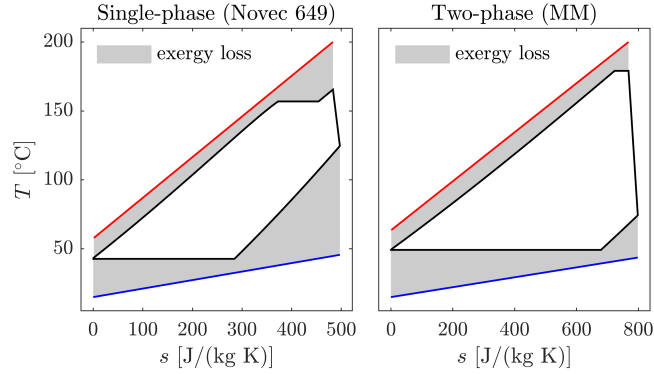


Figure 1: Comparison between an ORC operating with single-phase (left) and two-phase (right) expansion from an open heat source.

superheated vapour. This is an important distinction, which could have implications for the expander design.

Thus, there is sufficient evidence to suggest that the TFC, or cycles with two-phase expansion, can outperform a standard ORC. However, the main challenge associated with realising this is the identification of a suitable expander that can tolerate two-phase conditions. The continued work of Smith [3, 6] identified twin-screw expanders as one of the most promising technologies for such applications. A twin-screw expander is a positive-displacement expander, constructed from two helical lobed rotors that mesh together to form the working chamber, and being a positive-displacement machine means it is well suited to two-phase operating conditions. The interest in twin-screw expanders for this purpose is further evidenced by a number of further studies found within the literature [7, 8]. Twin-screw expanders are already employed within commercially available ORC systems [9], and are also used commercially for the expansion of wet steam [10]. However, one issue surrounding the use of twin-screw expanders is that twin-screw expanders are limited in their achievable expansion ratio by the built-in volume ratio of the machine. Thus, to efficiently operate with high volume ratios, it becomes necessary to consider multiple expansion machines, and even for a system using two expanders in series the overall volumetric expansion ratio may be limited to around 20 [11]. Thus, twin-screw expanders are only suitable for low-temperature applications, typically around 100 °C.

Therefore, to consider two-phase expansion in higher temperature applications it is necessary to consider other options. Scroll expanders are widely considered for ORC applications, but are only suitable for systems of a few kilowatts and below, although for higher power ratings multiple expanders connected in parallel could be considered. However, much like twin-screw expanders, scroll expanders may also be restricted in their achievable volume ratio, which would mean multiple machines in series would also be required to obtain the required expansion ratio. Reciprocating-piston expanders may also be a candidate, but limited prototypes have been developed, and those that have report low efficiencies [12]. In comparison, turboexpanders are widely used in ORC systems, and are compact, efficient, and capable of achieving large expansion ratios over a single stage. However, the high-speed flow within a turboexpander means that any liquid droplets present in the rotor will cause erosion due to liquid droplets impacting on the blade surface [13]. Therefore, most commercial turbines are not designed for two-phase conditions. Novel two-phase turbine designs have been investigated for expansion valve replacement [14], geothermal applications [15–17], and low-temperature power generation [18, 19], but these turbines are not widely implemented or may not be suitable for high-temperature applications. The performance of these machines is also relatively poor, with maximum nozzle isentropic efficiencies of 45% [19], and turbine isentropic efficiencies of 24% [20] being reported.

At this point, it is worth noting that any reduction in turbine efficiency will offset the thermodynamic benefit of two-phase expansion. Thus, it can be rationalised that for a two-phase ORC system to be competitive with single-phase systems, two-phase expander technologies must obtain similar isentropic efficiencies to existing single-phase expanders, which are typically in excess of 70%. Therefore, to realise competitive two-phase systems, innovations in cycle and turbine design are required. As previously noted, certain fluids, when operated within a two-phase ORC system, may transfer from being in a two-phase state to a superheated vapour during the expansion process [5]. Therefore, the first part of the expansion occurs under two-phase conditions, whilst the second part of the expansion process may occur under superheated conditions. Thus, if a suitable fluid can be selected, and the two-phase expansion region can be confined to the initial portion of the stator, it may be possible to design a suitable turboexpander to achieve two-phase expansion. This concept was explored in the 1980s by Elliott [21], who investigated various types of two-phase turbine, and referred to the cycle in question as a wet-to-dry cycle. Within that work, the expansion of toluene within a nozzle from an inlet temperature 289 °C and vapour quality of 1% to an outlet temperature of 70 °C was studied experimentally. The results indicated a nozzle efficiency, defined as the ratio of the kinetic power of the jet to the isentropic jet power, equal to 0.98, leading to Elliott concluding that the wet-to-dry cycle was perhaps the most attractive prospect for two-phase turbines. However, since that work very limited studies on this sort of turbine have been reported.

Given the need to enhance the performance of waste-heat recovery systems to ultimately facilitate a wider uptake of these technologies, the aim of this paper is to investigate the design of a two-phase ORC system operating with particular organic fluids that allow a wet-to-dry expansion across the turbine. Specifically, it is postulated that this could enable the power output from ORC systems to be increased by up to 30%, whilst allowing turbine designs with high isentropic efficiencies to be realised that are similar to existing single-phase turbines. To the author's knowledge, this paper is the first study of its kind to explore the thermodynamic simulation, optimisation and fluid selection for this type of cycle, and to extend existing mean-line design methods for single-phase ORC turbines to the design and optimisation of radial-inflow turbines operating with two-phase inlet conditions. The outcomes of this study include the identification of the most promising working fluids and optimal cycle operating conditions that achieve the targeted improvement in power output, and the generation of candidate two-phase turbine designs that can be developed further in later studies. An important consideration for the two-phase cycle, particularly given the target application of waste-heat recovery where heat-source conditions may fluctuate, is the off-design performance and the associated control strategy. This topic lies outside the scope of the current paper, but should be considered in future studies. In particular, the ability to monitor and determine the fluid conditions at the turbine inlet, and to ensure dry-vapour conditions at the rotor inlet is likely to represent a significant challenge.

## 2. Fluid candidates

During the design and optimisation of any ORC system it is important to consider a range of different fluid candidates for the working fluid within the cycle. However, for a two-phase ORC system in which expansion begins in the two-phase region and ends in the superheated region, it is even more important to select a suitable working fluid. In particular, fluids with a saturated-vapour line that has a positive slope, often referred to as 'dry' fluids, are required. A number of common ORC fluids are considered within this study and these are summarised in Tab.

1, along with their critical temperatures. This list includes hydrocarbons, siloxanes and two Novec fluids. The saturation curves for a subset of these fluids are reported in Fig. 2, as viewed in the temperature-entropy plane. Only a subset of the 12 fluids are shown to highlight the differences in the shape of the saturation curve and to give an indication of how this affects the feasibility of two-phase expansion.

Table 1: Working-fluid candidates.

Fluid	$T_{cr}$ [°C]	$p_{cr}$ [bar]	Fluid	$T_{cr}$ [°C]	$p_{cr}$ [bar]
<i>n</i> -propane	96.9	42.5	<i>n</i> -pentane	196.7	33.7
<i>iso</i> -butane	134.8	36.3	<i>cyclo</i> -pentane	238.7	45.7
R1233zd	165.8	35.7	MM	245.7	19.4
Novec649	168.8	18.7	benzene	289.0	49.1
<i>iso</i> -pentane	187.3	33.8	MDM	291.1	14.2
Novec774	195.4	17.1	toluene	318.7	41.3

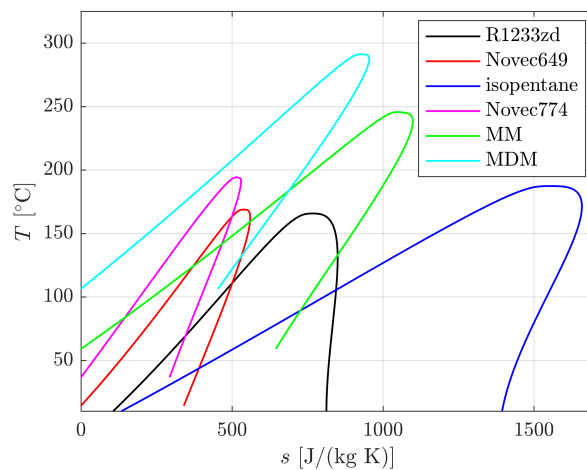


Figure 2: Saturation curves for the most promising fluid candidates viewed in the  $T$ - $s$  plane.

From observing Fig. 2, it is apparent that the Novec fluids and the siloxanes (MM and MDM) exhibit the characteristic ‘dry’ fluid shape, and thus these are likely to be promising candidates for the two-phase ORC system. Specifically, if one selects a point along the saturated-liquid line of one of these fluids that has a relatively high reduced pressure and extends an isentrope from that point, that isentrope will eventually enter the dry-vapour region. This would indicate that with these fluids an isentropic expansion from saturated liquid could feasibly end in the dry-vapour region. On the contrary, for R1233zd this is not possible at all, whilst for iso-pentane two-phase to dry-vapour expansion can only be realised for a sufficiently high expander inlet vapour quality. Thus, these fluids are unlikely to be suitable candidates for the two-phase system under consideration.

### 3. Thermodynamic modelling and optimisation

To identify the most promising fluid and thermodynamic cycle for the two-phase system a thermodynamic cycle model has been developed that couples thermodynamic analysis with a simple model of the turbine. The cycle is

shown in the temperature-entropy plane in Fig. 3, in which the notation used to describe the system is defined. Thermodynamic properties are computed using the thermodynamic models available within NIST REFPROP [22].

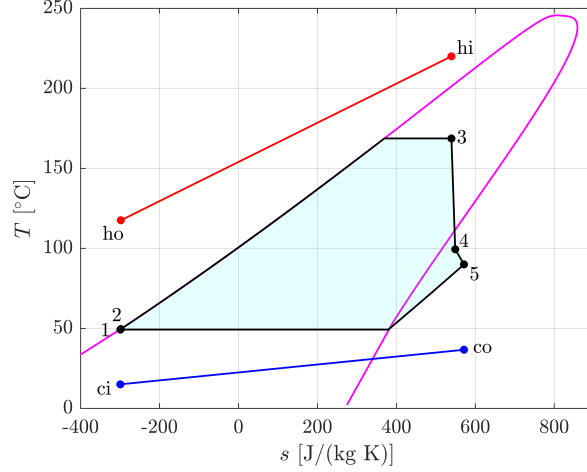


Figure 3: Notation used to describe the ORC system operating with two-phase expansion.

### 3.1. Cycle modelling

The cycle model has been developed to determine the power output that can be obtained from a fixed heat source and heat sink, both defined in terms of an inlet temperature, pressure and mass-flow rate. The cycle is assumed to operate under a steady-state condition, whilst pressure drops and heat losses are neglected. For this system there are four variables; namely the condensation temperature  $T_1$ , the reduced evaporation pressure  $p_r$  ( $p_2/p_{cr}$ ), the expander inlet condition  $x_3$ , and the non-dimensional heat-source temperature drop  $\theta$ , defined by:

$$\theta = \frac{T_{hi} - T_{ho}}{T_{hi} - T_{ci}}, \quad (2)$$

where  $T_{hi}$ ,  $T_{ho}$  and  $T_{ci}$  are the heat-source inlet, heat-source outlet and heat-sink inlet temperatures respectively. To avoid constraining the cycle to only two-phase cycles, the expander inlet condition  $x_3$  is defined in a way as to allow both single- and two-phase expansion. If  $x_3 \leq 1$ ,  $x_3$  is equal to the expander inlet vapour quality, whilst for  $x_3 > 1$ , the expander inlet temperature is found from:

$$T_3 = T_{3'} + (x_3 - 1)(T_{hi} - T_{3'}), \quad (3)$$

where  $T_{3'}$  is the evaporation saturation temperature and  $T_{hi}$  is the heat-source inlet temperature. Thus, by allowing  $x_3$  to range between 1 and 2 allows the turbine inlet temperature to range between  $T_3 = T_{3'}$  ( $x_3 = 1$ ) and  $T_3 = T_{hi}$  ( $x_3 = 2$ ). However, during an optimisation  $x_3 = 2$  will never be achieved due to a pinch-point constraint.

Based on  $T_1$ ,  $p_r$  and  $x_3$  all conditions at state points 1 and 3 follow from the equation of state. The pump and turbine are modelled by an assumed isentropic efficiency, denoted  $\eta_p$  and  $\eta_t$  respectively, which in turn leads to determination of all fluid properties at state points 2 and 5. The heat-source outlet temperature is provided from  $\theta$ , from which the heat-source enthalpy at the inlet and outlet can be obtained. An energy balance is then applied to

the heat-addition heat exchanger to determine the working-fluid mass-flow rate  $\dot{m}$ , before a final energy is applied to the heat-rejection heat exchanger to determine the heat-sink outlet temperature. With the cycle fully defined, the pinch points within each heat exchanger are calculated by discretising each heat exchange process into 10 segments, and a constraint is applied to ensure these remain above minimum allowed values. Thus, instead of considering  $T_1$  as a fixed input, during an optimisation the optimiser will seek the lowest condensation temperature that can be obtained that does not violate the pinch-point constraint in the condenser.

It is widely known that for waste-heat recovery applications it is advantageous to maximise net power output (which is equivalent to maximising the second-law efficiency), rather than cycle thermal efficiency. This is because maximising thermal efficiency could lead to an efficient cycle that does not fully exploit the available heat stream. Thus, the net power output is set as the objective function during the optimisation, which is defined as:

$$\dot{W}_n = \dot{m} [(h_3 - h_5) - (h_2 - h_1)] . \quad (4)$$

### 3.2. Preliminary turbine modelling

Within the turbine, the working fluid undergoes two expansion processes. Firstly, it is expanded within the stationary stator vane, before then expanding through the rotor. Given that the motivation is to confine two-phase conditions to the stator, it is prudent to determine the conditions at the inlet to the rotor, which, in turn, can be used to constrain an optimisation to ensure the rotor inlet conditions remain in the dry-vapour region. For this purpose, the degree of reaction is introduced:

$$R = \frac{h_4 - h_5}{h_3 - h_5} , \quad (5)$$

where  $h_3$ ,  $h_4$  and  $h_5$  are the enthalpies at the turbine inlet, rotor inlet and rotor outlet respectively. At this stage no distinction is made between total and static conditions at the turbine inlet and outlet (*i.e.*,  $h_3 = h_{03}$  and  $h_5 = h_{05}$ ), although  $h_4$  relates to static conditions. Alongside  $R$ , the stator isentropic efficiency  $\eta_n$  is introduced, which is directly related to the stator loss coefficient  $\zeta_n$ , and defined as follows:

$$\eta_n = \frac{1}{1 + \zeta_n} = \frac{h_3 - h_4}{h_3 - h_{4s}} , \quad (6)$$

where  $h_{4s}$  is the enthalpy at the rotor inlet following an isentropic expansion to the rotor inlet pressure  $p_4$ . The calculation procedure for the turbine can be summarised as follows. Firstly, based on the assumed turbine isentropic efficiency the conditions at the turbine inlet and outlet can be determined. Then,  $h_4$  and  $h_{4s}$  follow from Eqs. 5 and 6, which allows the rotor inlet conditions to be determined, since  $p_4 = f(h_{4s}, s_3)$ , and  $[T_4, \rho_4, x_4] = f(p_4, h_4)$ .

### 3.3. Heat-exchanger sizing

Heat-exchanger size is estimated through a discretised model that determines the product of the overall heat-transfer coefficient  $U$  and heat-transfer area  $A$ :

$$UA = \sum_{i=1}^n \frac{\dot{m}(h_{in,i} - h_{out,i})}{\Delta T_{\log,i}} , \quad (7)$$

where  $\dot{m}$  is the working-fluid mass-flow rate, and  $h_{\text{in}}$ ,  $h_{\text{out}}$  and  $\Delta T_{\text{log}}$  are the working-fluid inlet enthalpy, working-fluid outlet enthalpy, and counter-flow log-mean temperature difference of the  $i^{\text{th}}$  heat-exchanger element respectively. Since all parameters on the right-hand side of Equation 7 are provided by the thermodynamic model, this approach allows an estimate of the heat-exchanger size without requiring a detailed sizing model, or making order of magnitude assumptions for overall heat-transfer coefficients. Whilst this model is simple compared to others reported within the literature [23, 24], it allows the trade-off between power output and heat-exchanger size to be investigated through multi-objective optimisation and allows an assessment of whether two-phase cycles could have benefits for applications where maximising power output may not be the primary objective. However, this method does neglect differences in the heat-transfer coefficients owing to phase change. For the evaporator, which is found to make-up the majority of the total  $UA$  requirements and shows more variability than the condenser, this corresponds to the preheating and evaporation regions. However, within this study the heat source is considered to be a vapour and thus the heat-source heat-transfer coefficient will be significantly lower than the working-fluid heat-transfer coefficient during either preheating or evaporation. Thus, when the overall coefficient is considered there is not expected to a significant difference between the preheating or evaporating regions.

### 3.4. Cycle optimisation

Single- and multi-objective optimisation is applied within this study. The objective of the single-objective optimisation is to identify optimal cycles that maximise power from a defined heat source and heat sink. To allow a full exploration of potential solutions, all fluids reported in Tab. 1 are considered, and for each fluid, the optimisation is completed for three different degrees of reaction ( $R = 0.1, 0.3, \text{ and } 0.5$ ). The model has been implemented within MATLAB, and the optimisation is completed using the interior-point algorithm, which is a gradient-based optimiser available within the Global Optimisation Toolbox [25] that is suitable for constrained non-linear problems. The optimisation is repeated from 40 unique start points to ensure a global optimum is identified.

The heat-source and heat-sink conditions defined for the initial optimisation study are summarised in Tab. 2. The heat-source temperature is set to 200 °C, which is considered to be a temperature at which the concept developed in this paper could offer benefits over other ORC systems. At lower temperatures volumetric expanders could be a possibility to achieve two-phase expansion, whilst at higher temperatures the availability of working fluids with higher critical temperatures, and the associated increase in normal boiling temperature, could lead to supercritical systems or cascaded cycles being the preferred option. Nonetheless, following the initial study the effect of the heat-source temperature is investigated further. The heat source and heat sink are assumed to be air and water respectively, and since the optimal thermodynamic cycle is independent of the heat-source mass-flow rate, this is set to 1 kg/s; however, the optimal cycle will depend on the ratio of the heat-source and heat-sink heat-capacity rates,  $\tau$  (Equation 1). For the initial study the heat-sink mass-flow rate is set to 1 kg/s, which corresponds to  $\tau \approx 4$  considering the specific-heat capacities of air and water, although the effect of  $\tau$  is investigated later. The assumptions and optimisations bounds for the initial cycle optimisation are reported in Tab. 3. Although the upper bound for  $\theta$  is set to 1, this implies  $T_{\text{ho}} = T_{\text{ci}}$ , which cannot be achieved in practice. However, within the optimisation the possibility of this occurring is restricted by the pinch point constraint applied to both heat exchangers.

Following the single-objective optimisation a multi-objective optimisation is completed to assess the trade-off

Table 2: Defined heat-source and heat-sink conditions.

	Fluid	$T$ [°C]	$p$ [kPa]	$\dot{m}$ [kg/s]
Heat source	Air	200	101	1
Heat sink	Water	15	101	1

Table 3: Initial assumptions for the cycle optimisation study.

Pump isentropic efficiency	$\eta_p$	0.7	–
Turbine isentropic efficiency	$\eta_t$	0.8	–
Stator isentropic efficiency	$\eta_n$	0.9	–
Minimum pinch point	$PP_{\min}$	10	K
Rotor inlet constraint	–	$T_4 \geq T_4'$	–
Variables	–	min.	max.
Pump inlet temperature	$T_1$	25	80 °C
Reduced evaporation pressure	$p_r$	0.01	0.90 –
Expander inlet parameter	$x_3$	0	2 –
Heat-source temperature drop	$\theta$	0	1 –

between maximising the net power output and minimising the total heat-exchanger size (*i.e.*,  $UA_h + UA_c$ ) by generating the Pareto front. For a defined fluid and degree of reaction, the optimisation is completed for the same assumptions and bounds listed in Tabs. 2 and 3, although the minimum pinch-point is reduced to 2 K to evaluate the entire design space. The optimisation is completed using the genetic algorithm available within the Global Optimisation Toolbox [25], which is a variant of the non-dominated sorting genetic algorithm (NSGA-II).

### 3.5. Optimisation results

#### 3.5.1. Results for $T_{hi} = 200$ °C

After running the single-objective optimisation study, the optimal cycles that generate the maximum power were identified. To facilitate a comparison with an optimal ORC system operating with single-phase expansion, the optimisation was repeated for the same working fluids, but with the constraint  $x_3 \geq 1$  to ensure superheated vapour at the turbine inlet. Based on this, the optimal single-phase system was identified as one operating with Novec649 and this system has a net power output,  $\dot{W}_{\text{base}}$ , of 16.53 kW. To enable a complete comparison with state-of-the-art single-phase cycles, the optimisation was repeated for a recuperated single-phase cycle. However it was found that for the case of maximising power output, the addition of a recuperator did not enhance the power output from the single-phase cycle. This can be understood since the addition of a recuperator will enhance the first-law efficiency of the cycle, but it also increases the working-fluid temperature entering the heat-addition heat exchanger, which subsequently increases the heat-source outlet temperature leading to less recovery of the waste-heat stream.

To establish the effect of the working fluid and degree of reaction on the performance of the cycle a sample of the optimal cycles have been considered. Specifically, the 10 optimal two-phase cycles (out of 36) are reported in Fig. 4(a) in terms of the net power output and the optimal expander inlet vapour quality. Within this plot the power outputs are normalised by  $\dot{W}_{\text{base}}$  to establish the increase in power production when moving to two-phase expansion.

It is observed that the best two-phase system, operating with MDM, can generate 14.0% more power than the optimal single-stage system, thus reaffirming the performance improvement that is possible by utilising two-phase expansion. Changing to MM, Novec774, iso-pentane or Novec649 reduces this to 12.5%, 5.4%, 3.7%, 1.1% respectively.

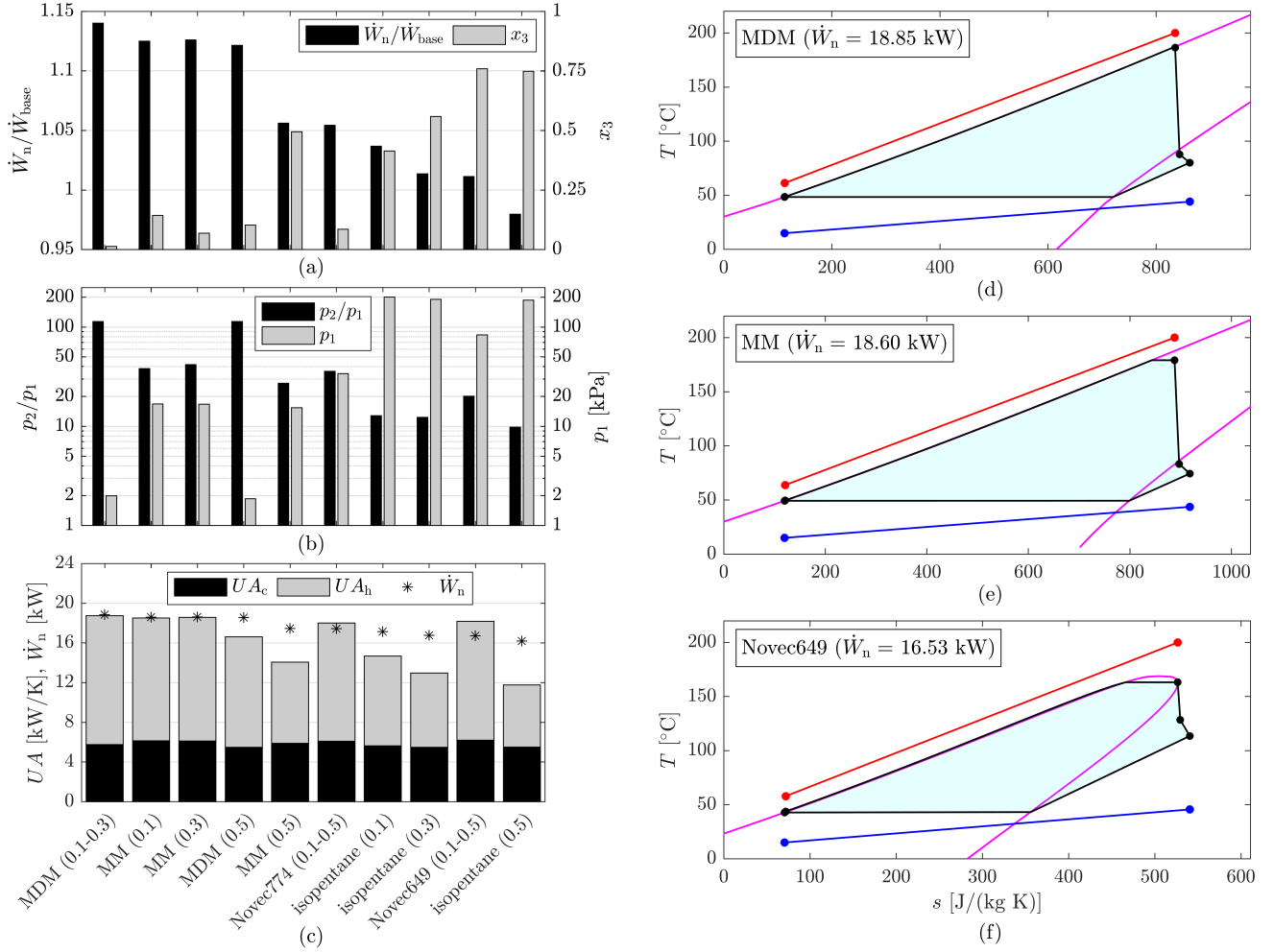


Figure 4: Results from the single-objective optimisation for the two-phase cycles with  $T_{hi} = 200$  °C; (a) optimal power output and expander inlet vapour quality; (b) optimal pressure ratio and condensation pressures; (c) heat-exchanger requirements; (d) optimal MDM two-phase cycle; (e) optimal MM two-phase cycle; (f) optimal base-line non-recuperated single-phase cycle with Novec649. In (a)-(c) the number in brackets after the working fluid refers to degree of reaction.

The results reported in Fig. 4(a) also indicate a correlation between reducing the expander inlet vapour quality and increasing the power output. This is because a lower vapour quality corresponds to a smaller amount of heat being transferred under isothermal conditions, and also leads to less superheat at the turbine outlet, which combined reduces the exergy loss within the heat-addition and heat-rejection process. The optimal two-phase cycles for MDM and MM, alongside the optimal base-line non-recuperated single-phase cycle, are reported in Figs. 4(d-f) in the form of temperature-entropy diagrams. From these plots, the reduced temperature differences in the heat-addition and heat-rejection processes can be readily observed, indicative of a reduction in the overall exergy loss within the cycle, and an increase in the second-law efficiency. Thus, from a thermodynamic perspective low vapour qualities are preferable. However, it is worth noting that reducing the vapour quality is likely to lead to a large change in density across the turbine, which may have implications for the turbine design and achievable turbine efficiency.

Alongside  $x_3$ , it is important to consider additional factors that may affect system design. Specifically, the pressure ratio,  $p_2/p_1$ , and condensation pressure,  $p_1$ , should be considered, which are reported for the optimal cycles in Fig. 4(b). The system pressure ratio will impact the turbine design, with large pressure ratios leading to possible

supersonic conditions within the stator or rotor, alongside contributing to the large change in density across the turbine. Moreover, low condensation pressures require the condenser to operate under a vacuum, whilst the large volumetric flow rate increases the physical size of the condenser. Referring to the optimal MDM case, the optimal pressure ratio is 113 whilst the condensation pressure is 2.0 kPa. However, shifting to using MM instead of MDM, the net power output is only reduced by  $-1.3\%$ , but the pressure ratio is reduced to 38, whilst the condensation pressure is increased to 16.8 kPa.

The heat-exchanger requirements are reported in Figure 4(c). For all the two-phase cycles, the condenser heat-exchanger requirements ( $UA_c$ ) do not vary significantly, ranging from 5.5 W/K for *iso*-pentane (0.3) to 6.2 W/K for Novec649 (0.1–0.5). In contrast, the variation in the evaporator requirements ( $UA_h$ ) is more significant ranging from 6.3 W/K for *iso*-pentane (0.5) to 13.0 W/K for MM (0.1–0.3), leading to the combined heat-exchanger requirements ( $UA_h + UA_c$ ) ranging from 11.6 W/K for *iso*-pentane (0.5) to 18.8 W/K for MM (0.1–0.3). Thus, the best performing cycle requires the largest heat-exchanger requirements and vice versa. Considering the ratio  $(UA_h + UA_c)/\dot{W}_n$ , which can be considered as a preliminary economic indicator that provides an indication of the amount of heat-exchange area required per unit power, this ranges between  $0.73 \text{ K}^{-1}$  for *iso*-pentane (0.5) and  $1.09 \text{ K}^{-1}$  for Novec649; for the cycles that generate the maximum power, namely MDM (0.1–0.3), MM (0.1) and MM (0.3), this ratio equal to  $1.00 \text{ K}^{-1}$ . This indicates that from the perspective of minimising the heat-exchanger requirements per unit power, the worst performing of the 10 cycles may be the best option. Finally, it is worth comparing the two-phase cycles to the heat exchanger requirements for the optimal single-phase cycle, which was obtained with Novec649. For this single-phase cycle, the total heat-exchanger requirements are estimated to be 17.7 W/K, which for a power output of 16.53 kW corresponds to a value for  $(UA_h + UA_c)/\dot{W}_n$  of  $1.07 \text{ K}^{-1}$ . Thus, these preliminary sizing results suggest that for a waste-heat recovery application where the objective is to maximise the power output, the proposed two-phase cycle not only leads to a higher power output than the optimal single-phase cycle, but also requires less heat-exchanger area per unit of power produced. However, a more detailed heat-exchanger sizing and techno-economic study will be required to further support this preliminary finding.

For the thermodynamic study the pump and turbine are modelled using a fixed isentropic efficiency. Moreover, for a fixed expansion process, the fluid state at the rotor inlet is related to the stator isentropic efficiency, and is constrained to ensure superheated vapour enters the rotor. Thus, a sensitivity study concerning these three isentropic efficiencies has been conducted, with the results reported in Fig. 5. These results reveal that the optimisation is insensitive to the assumed values for the pump and stator efficiencies. On the other hand, the turbine design is found to be more sensitive. Having said this, it is still observed that the same trends are observed with MDM and MM being the optimal fluids that result in maximum power.

Following the single-objective optimisation, the multi-objective optimisation was completed to assess the trade-off between thermodynamic performance and heat-exchanger requirements. Following the results reported in Fig. 4, the multi-objective optimisation was completed with MDM and MM, both with degrees of reaction equal to 0.1, 0.3 and 0.5, and these are compared with both recuperated and non-recuperated single-phase cycles operating with the 12 fluids listed in Tab. 1. The results from the study are reported in Fig. 6, and a sample of the optimal cycles taken from the Pareto fronts for the  $R = 0.1$  cases are reported in Fig. 7.

Comparing the Pareto fronts for the two-phase cycles, it is observed that the performance with both MDM and

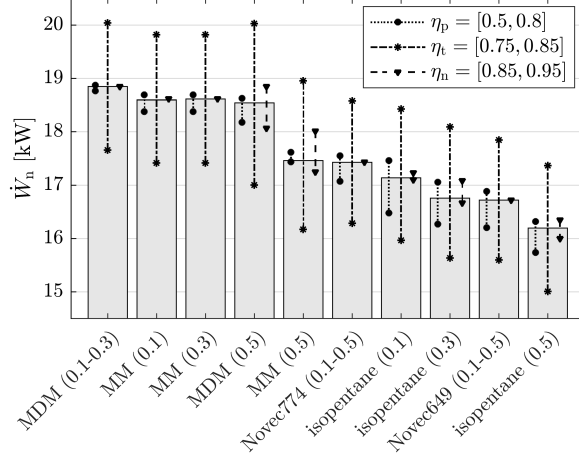


Figure 5: Sensitivity of the single-objective optimisation results to the isentropic efficiencies for the pump  $\eta_p$ , turbine  $\eta_t$  and stator  $\eta_n$ .

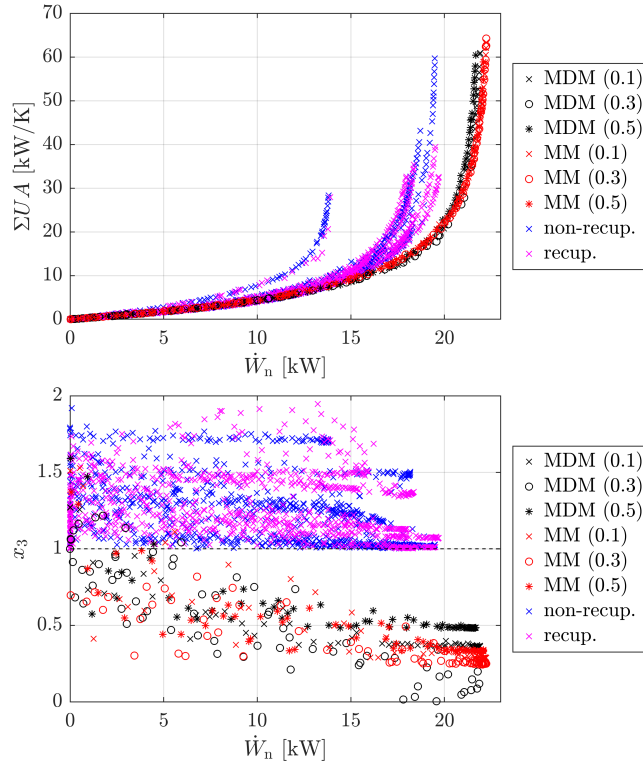


Figure 6: Results from the multi-objective optimisation for  $T_{hi} = 200$  °C; the top plot compares the Pareto fronts obtained for two-phase cycles operating with MDM and MM at different degrees of reaction to non-recuperated (non-recup.) and recuperated (recup.) single-phase cycles; the bottom reports the variation in the expander inlet parameter  $x_3$  across the Pareto fronts.

MM is very similar, indicating that either fluid would be a suitable for the two-phase expansion cycle. Moreover, for both fluids there appears to be no discernible difference between the Pareto fronts for the different degrees of reaction. This is because the shape of the saturation dome on a  $T$ - $s$  diagram has a large overhang for both fluids, meaning an expansion from a relatively low vapour quality can be easily obtained with any value of reaction. Although a lower degree of reaction may result in a lower achievable design-point efficiency for the turbine, which will be investigated in more detail in the following section.

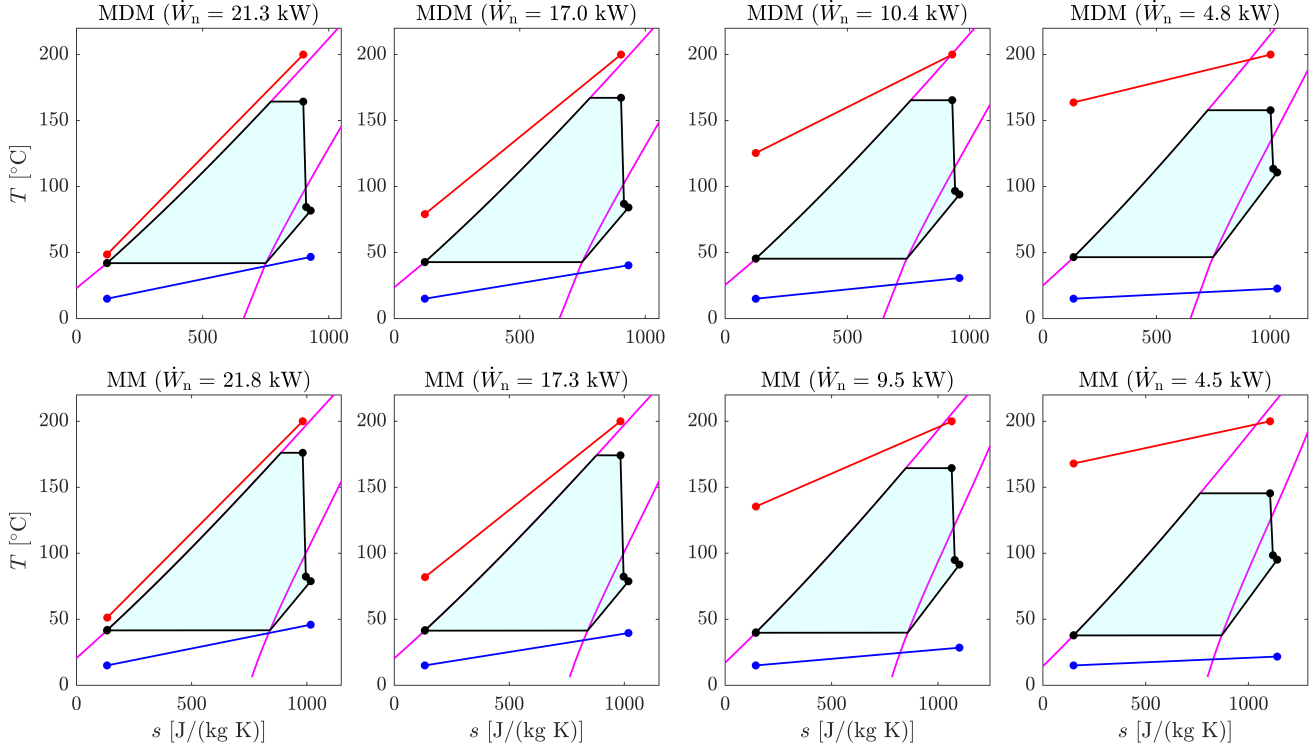


Figure 7: Representative optimal two-phase cycles shown on a  $T$ - $s$  diagram taken from the Pareto fronts obtained from the multi-objective optimisation. The top row corresponds to MDM with  $R = 0.1$ , and the bottom row corresponds to MM with  $R = 0.1$ .

Comparing the Pareto fronts for the single- and two-phase cycles, the two-phase cycles are found to consistently produce more power for the same heat-exchanger requirements than both the non-recuperated or recuperated single-phase cycles. Specifically, for combined  $UA$  values (*i.e.*,  $UA_h + UA_c$ ) of 10, 20, 40 and 60 kW/K the optimal two-phase cycles generates approximately 3.9%, 7.0%, 10.6% and 13.3% more power than the optimal single-phase cycle. In other words, two-phase cycles could generate more power for the same heat exchanger size, which suggests that two-phase cycles may have benefits across a broader range of applications than just applications where the objective is to maximise power. However, it is reiterated that more detailed investigations comprised of more sophisticated heat-exchanger models and a suitable economic assessment are needed to verify this finding.

Finally, considering the sample of optimal cycles reported in Fig. 7, the trends in the variation in the cycle parameters across the Pareto fronts can be observed. In particular, as a cycle with a higher power output is selected, the general trend indicates an increase in the evaporation pressure, a reduction in the expander inlet vapour quality and a reduction in the condensation temperature. However, more importantly, there is a significant reduction in the heat-source temperature drop, indicating that the heat source is not effectively utilised.

In summary, the thermodynamic optimisation suggests that MM and MDM are promising candidates for the two-phase expansion system. However, based on the lower pressure ratios and higher condensation pressures, MM may be a more suitable candidate from the component perspective, and is thus one of the most promising fluids for the heat-source and heat-sink conditions defined in Tab. 2. In Section 4, a parametric study on the effect  $x_3$  and degree of reaction on the cycle performance and turbine design will be completed considering only MM.

### 3.5.2. Results for different heat-source and heat-sink conditions

Before moving onto turbine design, a final study has investigated how two-phase cycles compare to single-phase cycles for different heat-source and heat-sink conditions. For this assessment, two additional heat-source temperatures, namely 150 and 250 °C, have been considered, in addition to two additional heat-sink mass-flow rates, namely 0.25 and 10 kg/s, which correspond to  $\tau \approx 1$  and  $\tau \approx 40$  respectively. In addition to maximising power, applications with a fixed heat-source temperature drop are also considered, defined by values of  $\theta$  equal to 0.1, 0.25 and 0.5. For each combination of heat-source temperature, heat-sink mass-flow rate and heat-source temperature drop the optimal single- and two-phase cycles have been identified. The results are summarised in Tab. 4, and have been generated considering non-recuperated single-phase cycles.

Table 4: Comparison of non-recuperated single- and two-phase cycles for a range of heat-source and heat-sink conditions. The percentages reported in brackets indicate a negative impact.

			Optimal single-phase			Optimal two-phase			Relative change		
$T_{hi}$	$\dot{m}_c$	$\theta$	$\dot{W}_n$	$UA$	$UA/\dot{W}_n$	$\dot{W}_n$	$UA$	$UA/\dot{W}_n$	$\Delta\dot{W}_n$	$\Delta UA$	$\Delta UA/\dot{W}_n$
[°C]	[kg/s]		[kW]	[kW/K]	[K <sup>-1</sup> ]	[kW]	[kW/K]	[K <sup>-1</sup> ]	[%]	[%]	[%]
150	0.25	-	4.12	4.55	1.10	4.18	4.37	1.04	+1.44	-3.81	-5.18
		1	7.41	8.23	1.11	9.48	13.94	1.47	+28.0	(+69.4)	(+32.4)
		10	10.41	14.83	1.42	13.31	18.63	1.40	+27.9	(+25.6)	-1.73
	1	0.1	2.38	1.74	0.73	2.38	1.74	0.73	-	-	-
		0.25	5.19	3.73	0.72	5.19	3.73	0.72	-	-	-
		0.5	7.27	6.98	0.96	7.71	7.27	0.94	+6.00	(+4.16)	-1.73
200	0.25	-	8.49	10.16	1.20	9.01	10.73	1.19	+6.07	(+5.64)	-0.40
		1	16.53	17.74	1.07	18.85	8.76	1.00	+14.0	(+5.71)	-7.28
		10	21.95	21.66	0.99	25.22	25.27	1.00	+14.9	(+16.7)	(+1.57)
	1	0.1	4.04	2.08	0.51	4.04	2.08	0.51	-	-	-
		0.25	9.19	4.45	0.48	9.19	4.45	0.48	-	-	-
		0.5	14.42	8.80	0.61	14.42	8.80	0.61	-	-	-
250	0.25	-	13.52	8.20	0.61	13.71	8.35	0.61	+1.46	(+1.81)	(+0.35)
		1	27.48	19.65	0.72	28.38	23.03	0.81	+3.29	(+17.2)	(+13.5)
		10	37.20	26.84	0.72	37.69	27.76	0.74	+1.30	(+3.42)	(+2.10)
	1	0.1	5.81	2.32	0.40	5.81	2.32	0.40	-	-	-
		0.25	13.59	5.01	0.37	13.59	5.01	0.37	-	-	-
		0.5	22.66	9.35	0.41	22.79	9.74	0.43	+0.56	(+4.23)	(+3.65)

From these results, it is observed that for all applications where the objective is to maximise power output, two-phase cycles outperform the single-phase cycles. For a restricted heat sink ( $\tau \approx 1$ ), the benefit is small (<6%), but increases to a maximum of 28% for  $\tau \approx 4$  and  $\tau \approx 40$ . Moreover, the performance benefit deteriorates as the heat-source temperature increases, to the extent that the benefit reduces from a maximum of 28% for  $T_{hi} = 150$  °C to a maximum of 3% for  $T_{hi} = 250$  °C. Thus, providing that heat sink is sufficiently large, and the heat-source temperature is below 250 °C, a performance benefit can be expected. For applications where applications may not be the primary objective (*i.e.*, fixed  $\theta$ ), there doesn't appear to be a benefit in two-phase operation. Finally, the optimised two-phase cycles generally have larger heat-exchanger requirements, but in four of the six maximum power applications for  $T_{hi} = 150$  °C and 250 °C they have lower values for  $UA/\dot{W}_n$ .

Extending the comparison to recuperated single-phase cycles, it was again found that in applications where there is no constraint on  $\theta$ , the addition of a recuperator does not lead to an increase the power output. Thus, this confirms that two-phase cycles could outperform state-of-the-art single phase cycles in applications where large heat-source temperature drops are feasible.

#### 4. Mean-line turbine design

The turbine for the two-phase ORC system is assumed to be a radial-inflow turbine, which is capable of obtaining the required expansion over a single stage, and thus the two-phase and single-phase expansion regions can be readily divided across the stator and rotor respectively. Following the cycle optimisation, the next step is to investigate how two-phase operation, and more specifically, the expander-inlet vapour quality and degree of reaction affect the design of the turbine. A schematic of the turbine and the notation used to describe it is reported in Fig. 8.

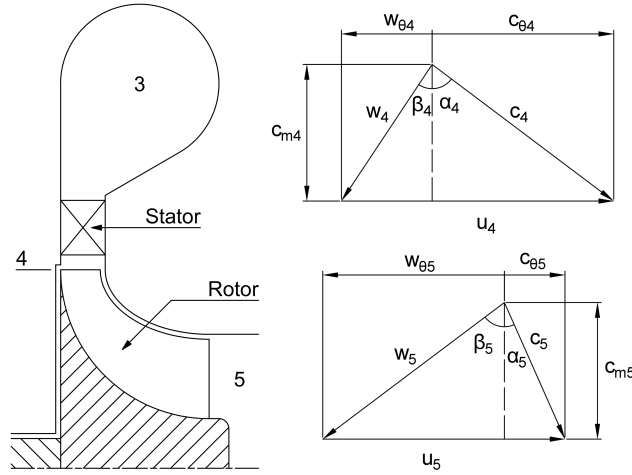


Figure 8: Notation used to define the radial turbine design.

##### 4.1. Motivation and the validity of the mean-line formulation for two-phase turbines

While the turbine rotor operates with a single-phase vapour, and thus existing mean-line models should be applicable, there is expected to be a significant uncertainty in modelling the stator. This is due to the large change in density, the low speed of sound of organic fluids, the strong likelihood of supersonic flow conditions, in addition to the uncertainty in the behaviour and interaction of the liquid and vapour phases (*i.e.*, the extent to which they are at mechanical and thermal equilibrium). Thus, the identification of an optimal cycle and turbine is a multi-faceted problem requiring a combination of cycle optimisation, mean-line design and numerical simulation under the most realistic operating conditions (*i.e.*, in-homogeneous and thermal non-equilibrium). Given that this topic has not been explored in detail before it is unrealistic to cover all of these aspects in this study. However, it is necessary to define a suitable starting point. Therefore, the motivation here is to identify base-line turbine geometries that can be studied in more detail in later studies, and for this purpose the mean-line formulation is considered appropriate.

Thus, to obtain these base-line geometries a mean-line model has been developed to assess important design parameters including the turbine dimensions, rotational speed, Mach numbers and the achievable isentropic efficiency of the turbine. Mean-line loss models have been readily developed and applied to the design of single-phase ORC radial-inflow turbines [26–28], but such methods have not, to the author’s knowledge, been applied to the design of two-phase turbines. However, it is rationalised here that providing that the fluid transitions from a two-phase fluid to a superheated vapour within the stator, such that the rotor operates entirely in the superheated vapour region, existing loss models for the rotor should remain valid.

For the two-phase stator, existing mean-line loss models, which are generally able to account for Mach and Reynolds number effects, could be applied if it is assumed that the two-phase fluid is homogeneous (*i.e.*,  $c_L = c_V$ ) and that the two phases are at thermal equilibrium (*i.e.*,  $T_L = T_V = T_{\text{sat}}$ ). This means there is a single mass, energy and momentum equation for the two-phase fluid, which could permit the mean-line loss models developed for single-phase fluids to be extended to two-phase operation. However, given that existing correlations were not developed for such applications, and that in the absence of any previous experimental or numerical studies relating to two-phase stator vanes there is no means to verify existing loss models for two-phase inlet conditions, it is unsuitable to rely completely on these models. Thus, to investigate their suitability, the performance of a number of candidate stator designs were initially evaluated using computational-fluid dynamics (CFD). To be consistent with the assumptions made within the mean-line approach, these simulations were completed assuming a homogeneous two-phase fluid under thermal equilibrium. Upon comparing the results a large discrepancy between the CFD and mean-line predictions was found, although a correlation for the stator loss coefficient was identified. The use of this correlation is deemed more suitable than either applying existing stator mean-line models, or assuming a constant stator loss coefficient which would fail to account for the possible effect of degree of reaction on the stator performance.

In summary, the mean-line formulation relies on a correlation derived from preliminary CFD simulations to model the stator performance, and existing mean-line loss models to model the rotor. More details on both are provided in the following subsections. This formulation allows preliminary turbine geometries to be obtained, which can be later studied using more sophisticated CFD models that account for non-equilibrium effects. Thus, it is clearly stated here that: (i) caution should be taken in extrapolating the correlation developed beyond the boundary conditions of this study; and (ii) that further studies are a necessity to evaluate the realistic performance of two-phase stator vanes.

#### 4.2. Mean-line radial turbine design

For brevity, the details of the mean-line model are reported in Appendix A, and only an overview of the model is given here. In summary, the turbine mean-line design is completed from the thermodynamic conditions identified during the cycle optimisation in addition to the assumed degree of reaction  $R$ . Alongside this, a number of turbine design variables and fixed design parameters are introduced as listed in Tab. 5. The design variables are subsequently optimised using the same gradient-based optimiser applied to the single-objective thermodynamic optimisation. For each set of design variables the design process is initiated with initial guesses for the isentropic total-to-static efficiency  $\eta_{ts}$  and stator isentropic efficiency  $\eta_n$ . Once the velocity triangles and turbine dimensions are established using the input variables, the stator and rotor loss coefficients are evaluated and the estimates for  $\eta_{ts}$  and  $\eta_n$  are updated. This is repeated until convergence. The constraints for the optimisation are listed in Tab. 5. Specifically, the rotor diameter ratio  $d_{5s}/d_4$  and blade angles are restricted to avoid excessive curvature of the blade, the relative Mach numbers within the rotor are constrained to ensure subsonic flow, the rotor inlet blade-height is restricted to be greater than 1 mm for manufacturability, and a maximum blade angle of  $45^\circ$  is permitted at the rotor inlet.

Within the mean-line model a critical aspect is the prediction of the rotor and stator loss coefficients. The rotor loss coefficient is computed using loss models for the passage, trailing-edge, post-expansion, clearance and disc friction losses. These models are identical to those reported in Ref. [28], with the omission of incidence loss since the current study deals only with design-point performance. The stator loss coefficient is discussed in the next section.

Table 5: Fixed and variable design inputs and constraints for the design optimisation of the two-phase radial-inflow turbine.

Design variables		min.	max.	units
Loading coefficient	$\psi = \Delta h_0/u_4^2$	0.50	2.00	-
Flow coefficient	$\phi = c_{m5}/u_4$	0.05	0.50	-
Meridional velocity ratio	$\xi = c_{m4}/c_{m5}$	0.80	1.20	-
Rotor diameter ratio	$\varepsilon = d_{5,rms}/d_4$	0.55	0.63	-
Hub/shroud ratio at outlet	$\lambda = d_{5h}/d_{5s}$	0.40	0.70	-
Fixed design parameters				
Number of rotor blades	$Z_r$	11	-	-
Rotor clearance gap	$\delta_{c1}$	0.20	mm	-
Axial length ratio	$L/d_4$	0.30	-	-
Optimisation constraints				
Shroud/inlet diameter ratio	$d_{5s}/d_4$	$\leq 0.85$	-	-
Inlet relative Mach number	$Ma_{4'}$	$\leq 1$	-	-
Outlet relative Mach number	$Ma_{5'}$	$\leq 1$	-	-
Inlet blade height	$b_4$	$\geq 1$	mm	-
Inlet relative flow angle	$\beta_4$	$\leq 45$	°	-
Inlet absolute flow angle	$\alpha_5$	$\leq 80$	°	-
Outlet relative flow angle	$\beta_5$	$\leq 75$	°	-
Outlet absolute flow angle	$ \alpha_5 $	$\leq 20$	°	-

The rotor design model has been validated against the results reported in Ref. [29], in which eight optimal radial-turbine designs for a 15 kW ORC system were generated, with each design corresponding to a different working fluid. Using the same inputs, the current model predicts values for the total-to-total and total-to-static efficiencies that agree to within 1.5% (relative), and rotor diameters that agree within 3%. The deviation in the rotor diameter is attributed to slight differences in the treatment of blockage in the two models, but nonetheless, the results are deemed sufficiently close for the purpose of this study. Full details of the comparison are reported in Tab. 6.

### 4.3. Stator loss investigation

As noted previously, existing stator loss models are not expected to be suitable for predicting the performance of a stator vane in which the working fluid transitions from being a two-phase fluid to a superheated vapour within the stator passage. Instead, a number of candidate stator designs have been assessed through preliminary CFD simulations. For this initial assessment it is assumed that the stator operates under full admission, whilst the nozzle is a planar nozzle with a passage width that is equal to the rotor inlet blade height. Further details on the stator design methodology studies are summarised in Appendix A.

Within the simulations, the two-phase fluid is modelled as a homogeneous two-phase fluid under thermal equilibrium and the stator loss coefficient between the stator inlet and rotor inlet radius is obtained. It is worth re-emphasising that the assumption of homogeneity and thermal equilibrium is an oversimplification and more detailed investigations into the two-phase expansion of organic fluid under realistic ORC operating conditions are a necessity to assess the influence of inhomogeneity and non-equilibrium. Nonetheless, for a preliminary study investigating the feasibility of the concept, the approach adopted here is considered to be appropriate to provide an initial indication of the loss coefficient through a CFD simulation that captures the stator loss mechanisms that are analogous to a single-phase ORC turbine (*i.e.* shock, trailing-edge and passage losses). It is also worth noting that wetness losses, which are known to be important in wet-steam expansion, are neglected in the current investigation.

Table 6: Validation of the rotor mean-line design model against Ref. [29].

		R245fa	R134a	R123	R236ea	R152a	R236fa	<i>n</i> -pentane	<i>iso</i> -butane
$T_{03}$ [K]		381.7	333	391.2	389.8	333	359.9	419	362.2
$p_{03}$ [kPa]		1527	1677	1155	2224	1497	1454	1478	1610
$p_5$ [kPa]		469.2	609.8	295.5	545.6	749.7	304.6	686.8	786.1
$\dot{m}$ [kg/s]		0.844	0.850	0.763	0.850	0.789	0.766	0.634	0.646
$\psi$		1.034	1.064	1.072	1.041	1.004	1.181	1.079	1.215
$\phi$		0.265	0.236	0.236	0.223	0.237	0.260	0.225	0.248
$\xi$		0.660	0.660	0.660	0.663	0.660	0.660	0.685	0.660
$\varepsilon$		0.752	0.712	0.739	0.730	0.741	0.741	0.733	0.757
$\lambda$		0.8	0.7	0.7	0.7	0.7	0.7	0.7	0.8
$Z_r$		18	20	20	21	19	20	21	21
$\eta_{ts}$ [29]		82.91	83.17	83.36	82.89	84.00	82.92	83.71	83.82
$\eta_{ts}$ [%]	current	81.95	83.91	83.42	83.37	82.73	83.60	83.52	83.67
	$ \Delta $ %	1.16	0.89	0.07	0.58	1.51	0.82	0.23	0.18
$\eta_{tt}$ [29]		85.45	85.04	85.21	84.54	86.02	85.05	85.37	85.75
$\eta_{tt}$ [%]	current	84.31	85.79	85.27	85.04	84.69	85.66	85.19	85.49
	$ \Delta $ %	1.33	0.89	0.07	0.59	1.54	0.72	0.21	0.31
$N$ [29]		38,502	43,439	35,160	43,124	40,574	36,029	43,430	39,849
$N$ [rpm]	current	37,540	42,649	33,904	41,920	39,153	35,395	42,101	38,965
	$ \Delta $ %	2.50	1.82	3.57	2.79	3.50	1.76	3.06	2.22
$d_4$ [29]		65.00	56.60	73.60	57.70	64.80	68.30	65.10	66.30
$d_4$ [mm]	current	66.36	58.14	75.77	59.47	66.60	69.76	67.08	67.75
	$ \Delta $ %	2.09	2.72	2.95	3.06	2.78	2.13	3.03	2.19
$b_4$ [29]		3.90	5.10	4.80	3.70	5.70	4.00	5.30	5.10
$b_4$ [mm]	current	4.08	5.34	4.94	3.76	5.87	4.34	5.49	5.44
	$ \Delta $ %	4.65	4.64	2.95	1.66	3.01	8.43	3.63	6.58
$d_{5,rms}$ [29]		48.90	40.30	54.40	42.10	48.00	50.60	47.70	50.20
$d_{5,rms}$ [mm]	current	49.90	41.40	56.00	43.41	49.35	51.69	49.17	51.29
	$ \Delta $ %	2.05	2.72	2.94	3.11	2.81	2.15	3.07	2.17
$b_5$ [29]		6.80	8.30	8.80	7.20	7.50	8.00	7.70	6.50
$b_5$ [mm]	current	6.96	8.56	9.11	7.43	7.71	8.17	7.96	6.74
	$ \Delta $ %	2.39	3.15	3.48	3.19	2.74	2.14	3.43	3.64
$\alpha_4$ [29]		79.90	81.44	81.55	82.00	80.90	81.35	81.90	82.00
$\alpha_4$ [°]	current	80.13	81.49	81.56	81.86	80.93	81.54	81.75	82.18
	$ \Delta $ %	0.28	0.06	0.01	0.17	0.04	0.23	0.18	0.22
$\beta_5$ [29]		72.20	72.47	72.91	72.70	73.00	72.21	72.90	73.00
$\beta_5$ [°]	current	71.47	72.40	72.95	73.32	72.95	71.47	73.39	72.53
	$ \Delta $ %	1.00	0.09	0.05	0.85	0.06	1.03	0.68	0.64

The four candidate stator designs considered are summarised in Tab. 7. These have been developed for the two-phase expansion of MM from different turbine inlet pressures and vapour qualities. In each case, the degree of reaction is set to the maximum degree of reaction that allows the expansion to transition across the two-phase region, whilst an assumption for the rotor inlet radius and absolute flow angle is made. Following loss models developed for single-phase stator vanes, it is expected that, alongside variations in the Mach number, the stator loss coefficient will be affected by the Reynolds number at the stator outlet, which in turn depends on the passage blade height [28, 30]. Thus, to investigate this each stator design is simulated at the design passage height, and at passage heights of 2 mm and 5 mm. In total, this leads to 12 stator designs that are evaluated through CFD simulations. Based on the stator mean-line design, the rotor inlet absolute Mach numbers are predicted to range between 1.7 and 2.2, whilst

the Reynolds numbers based on stator chord length ( $\rho_4 c_4 C_n / \mu_4$ ) range between  $5.8 \times 10^6$  and  $1.5 \times 10^7$  and the Reynolds number based on passage height ( $\rho_4 c_4 b_4 / \mu_4$ ) range between  $1.3 \times 10^5$  and  $7.7 \times 10^5$  respectively.

Table 7: Stator design parameters.

	Design				
	1	2	3	4	
fluid	MM				–
$p_{03}$	500	500	1000	1000	kPa
$q_{03}$	0.3	0.5	0.1	0.5	–
$R$	0.1	0.4	0.1	0.4	–
$\dot{m}$	0.535	0.472	0.401	0.346	kg/s
$\alpha_4$	75				°
$r_4$	100				mm
$b_4$	6.407	2.978	3.974	1.496	mm
$r_A / r_4$	1.1				–
$Z_n$	16				–
$C_n / o_{th}$	30	20	30	20	–
$o_{th}$	1.872	3.993	1.097	3.102	mm

The performance of each stator vane is assessed through a steady-state three-dimensional viscous simulation completed using ANSYS CFX (version 18). The two-phase fluid is modelled as a homogeneous fluid by defining a homogeneous binary mixture from look-up tables generated for the two-phases using the Span-Wagner multi-parameter equation of state for MM [31]. Using a homogeneous binary mixture means properties within the saturation dome are defined as the mass-fraction weighted sum of saturated liquid and vapour properties. Thus, as a first step, this permits the extension of the use of ANSYS CFX, which has been already been readily applied to the simulation of supersonic single-phase ORC turbines [32, 33], to two-phase turbines whilst still only solving a single mass, energy and momentum equation. The inlet boundary condition is defined by the turbine inlet total pressure, and corresponding saturation temperature, and the inlet vapour mass fraction. The outlet of the domain is positioned at the rotor inlet radius and the outlet boundary condition is defined using an average pressure value which is set to the design rotor inlet static pressure. A periodic boundary is applied, and as such only a single stator passage is simulated. Finally, in-line with previous studies considering ORC turbines [34, 35] the Spalart-Allmaras turbulence model is applied. It was not possible to sufficiently resolve the boundary layer and achieve sufficient mesh quality, so wall functions are applied and the mesh resolved such that  $y^+ \approx 25$ .

To assess the performance of each stator, the averaged stator loss coefficient is determined from:

$$\zeta_n = \frac{\bar{h}_4 - \bar{h}_{4s}}{\frac{1}{2} \bar{c}_4^2}, \quad (8)$$

where  $\bar{h}_4$  and  $\bar{h}_{4s}$  are the averaged enthalpy and isentropic enthalpy at the outlet domain, obtained from the mass-averaged temperature and pressure and the inlet entropy, and  $\bar{c}$  is the area-averaged absolute velocity.

Grid independence studies were completed for the first and fourth stator designs. For each design, four meshes with approximately 0.8, 1.7, 2.9 and 4.5 million elements were generated. For both cases the results for the mass-flow rate, outlet properties and loss coefficient obtained using the meshes with 2.9 million elements agreed to within 0.6% of the finest meshes. The final meshes have 50 elements in the spanwise direction and approximately 58,000 in the blade-to-blade region. Meshes of equivalent size were generated for the other stator designs.

For each stator design the CFD simulation was run at the design passage height, and at passage heights of 2 mm and 5 mm, and the performance of the stator vane assessed. Representative flow fields predicted from the CFD simulation are reported in Fig. 9, in which contours of vapour mass fraction, Mach number and static entropy at the midspan are reported for Case 1 ( $p_{03} = 500$  kPa;  $q_{03} = 0.3$ ;  $b_4 = 1.496$  mm). To ensure the consistent treatment of the fluid properties in both the two-phase and superheated regions the variation in thermo-physical properties was also investigated for all cases; specifically, there was no indication of a reduction in entropy or any variations in total enthalpy which are signs of an incorrect thermodynamic model. The Mach number contours are generated using the built-in model within CFX that obtains the two-phase speed of sound based on the volume-weighted sum of the acoustic impedances of the vapour and liquid components. This model neglects the effect of mass exchange on the two-phase speed of sound, but does avoid discontinuities in the speed of sound at the boundary between the two-phase and superheated vapour regions.

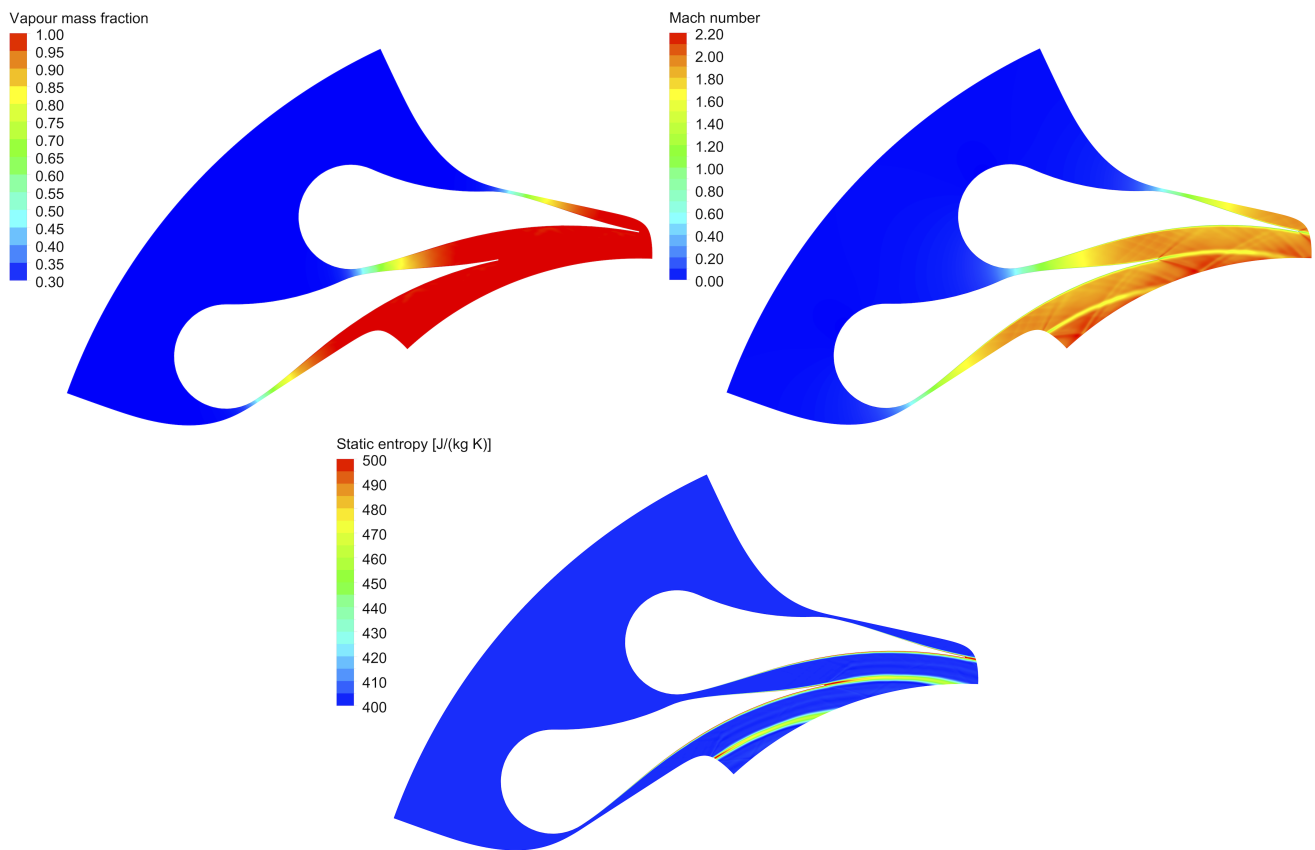


Figure 9: Contours of mid-span mass fraction, Mach number and static entropy for Case 1 ( $p_{03} = 500$  kPa;  $q_{03} = 0.3$ ;  $b_4 = 1.496$  mm).

The first thing to note from Fig. 9 is that these initial simulations indicate that a full transition from saturated two-phase conditions to superheated vapour is obtained after approximately two-thirds of the diverging section of the nozzle, providing initial indication of the feasibility of the concept explored in this paper. Secondly, the Mach number and static entropy contours are typical of the flow fields observed for single-phase supersonic ORC turbines, although the presence of an oblique shock pattern in the diverging portion of the nozzle would indicate there is room for further optimisation of the nozzle design. However, this was to be expected given the rather preliminary

stator design method employed.

It is worth reiterating that the stator is assumed to operate under full admission, whilst the stator passage height is equal to the rotor inlet blade height. Subsequently, given the high fluid density of at the turbine inlet, the velocity of the fluid at the leading-edge of the stator vane is low. Specifically, the area-averaged values obtained from the CFD simulations range between 0.5 m/s (Case 3) and 3.3 m/s (Case 2), and these correspond to the largest and smallest expansion ratios respectively. Thus, low inlet velocities are associated with the cases with the highest expansion ratios, and this could introduce challenges around achieving a uniform and homogeneous distribution of the two-phase fluid entering the stator. This requires further investigation, but potential options to mitigate this issue could include moving towards a partial-admission design, or using a non-planar nozzle. These options are associated with their own impact on the turbine design, either in terms of a partial-admission loss, or an increased complexity in manufacturing, but nonetheless these options could be considered in future studies if required.

After evaluating the performance of each stator design, a correlation between  $b_4$  and stator loss coefficient was observed, as reported in Fig. 10. This suggests that despite the average Mach numbers at the stator outlet domain varying between 1.5 and 2.1, for which a variation in shock losses would be expected, one of the most significant factors that affects the loss coefficient within the context of this study is the passage height, which is equal the rotor inlet blade height  $b_4$ . The CFD results have been fitted using a power law of the form:

$$\zeta_n = 0.5767b_4^{-0.8351} . \quad (9)$$

The corresponding value of  $R^2$  for Eq. 9 is 0.8864. Although caution should be made when extrapolating any correlation, a power law is preferential here to a linear correlation which could lead to  $\zeta_n < 0$  at high passage heights, or a polynomial which could exhibit spurious behaviour outside of the considered range. Finally, to investigate the sensitivity of the results to this correlation, an arbitrary shift of  $\pm 0.05$  has been considered within the following section; these curves are also reported in Fig. 10.

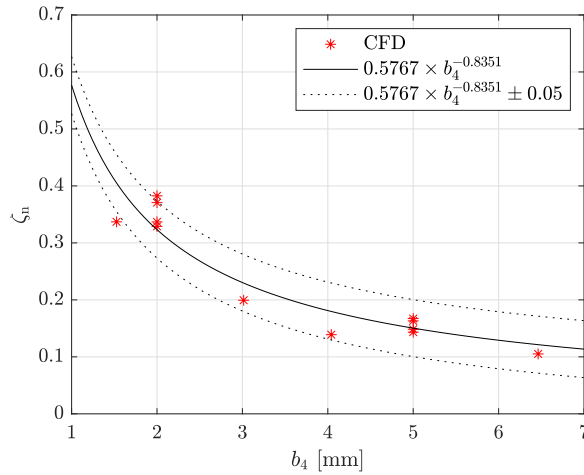


Figure 10: Relationship between passage height  $b_4$  and stator loss coefficient  $\zeta_n$  obtained using CFD for the four stator designs.

#### 4.4. Parametric optimisation study for MM

Having identified that MM is a suitable fluid for the two-phase ORC system, a detailed parametric cycle optimisation study considering this fluid has been conducted for the  $T_{hi} = 200$  °C and  $\dot{m}_c = 1$  kg/s case. The aim of this study is to evaluate the effect of the degree of reaction and expander inlet vapour quality on both the cycle and the turbine. For a range of values for  $R$  and  $x_3$  the cycle optimisation described in Section 3 has been repeated to find the optimal cycles that generate the maximum power and these results are reported in Fig. 11(a). From these results it is observed that a maximum power is obtained for  $x_3 = 0.1$  and a low degree of reaction ( $R < 0.4$ ). Accordingly, the maximum power is 18.6 kW, which is 12.5% more than the baseline single-phase system, and is the same result identified in Section 3.5. Furthermore, as long as  $R < 0.4$ , the power is independent of the degree of reaction. This is observed since the shape of the saturation dome of MM, when viewed in the  $T$ - $s$  plane, is sufficiently overhung such that only a small portion of the total expansion process takes place in the two-phase region within the optimal cycle. Thus, a higher degree of reaction can be selected without incurring any performance penalty. However, reducing  $x_3$  leads to a more significant reduction in the power output, and  $x_3$  should be less than 0.7 to generate more power than the baseline single-phase system.

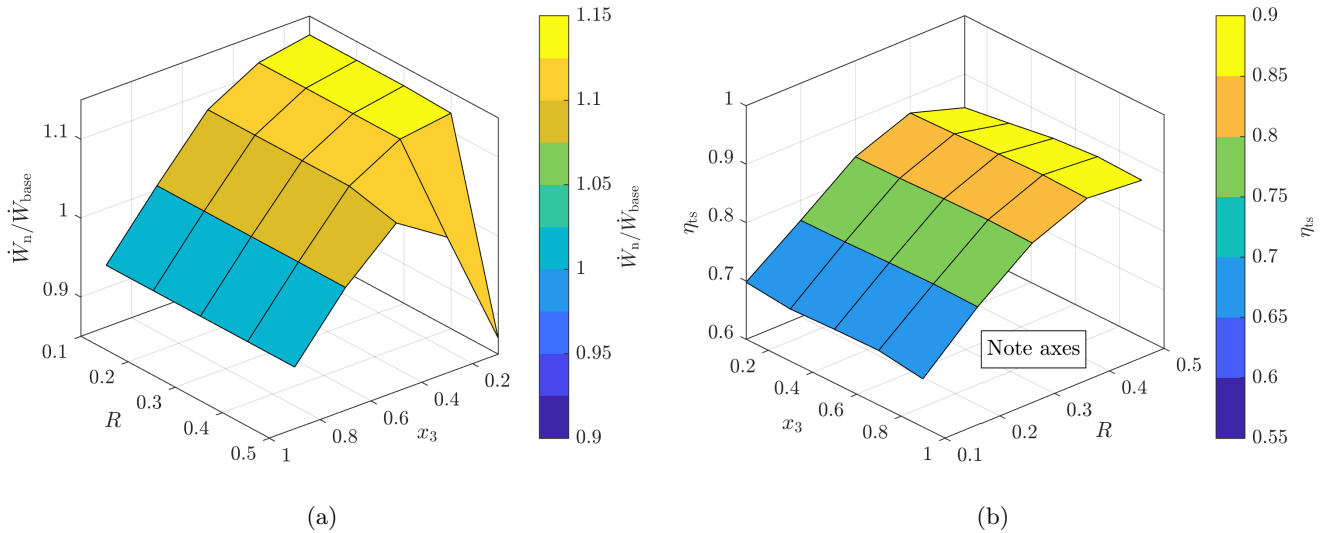


Figure 11: Effect of turbine inlet vapour quality and degree of reaction on the performance of the two-phase system operating with MM: (a) power output predicted by thermodynamic cycle where at each point the optimal cycle conditions are obtained using the cycle model reported in Section 3 assuming a fixed turbine efficiency; (b) optimal total-to-static isentropic efficiency obtained from the mean-line turbine design optimisation. Note that for visualisation purposes the axes in (b) have been flipped.

Following the cycle optimisation study, the turbine model was used to obtain an optimised turbine design for each cycle. The turbine total-to-static isentropic efficiency  $\eta_{ts}$  for each cycle is reported in Fig. 11(b). The first observation is that  $\eta_{ts}$  deteriorates significantly as the degree of reaction is reduced from 0.4 to 0.1, but does not vary significantly as the expander inlet vapour quality is reduced. This suggests that for a particular cycle the turbine should be designed with the maximum degree of reaction that is possible whilst ensuring that single-phase vapour is entering the rotor. Secondly, it is observed that the selection of the optimal cycle requires a combined consideration of both the thermodynamic performance of the cycle and the efficiency of the turbine. When doing so, the optimal operating point is found at  $x_3 = 0.1$  and  $R = 0.4$ , which corresponds to a power output (predicted from the cycle analysis) of 18.6 kW and  $\eta_{ts} = 87.2\%$ . It is worth noting here that the corresponding efficiencies are relatively high,

which could be associated with some uncertainty within the stator loss coefficient. As a preliminary assessment of this uncertainty the optimisation was repeated with different forms of the stator loss coefficient (as reported in Fig. 10). Specifically, it was found that a change in  $\zeta_n$  of  $\pm 0.05$  led to average changes in  $\eta_{ts}$  of  $-2.1\%$  ( $+0.05$ ) and  $+2.2\%$  ( $-0.05$ ) within the  $x_3$ - $R$ - $\eta_{ts}$  contour, with standard deviations of  $0.45\%$  ( $+0.05$ ) and  $0.51\%$  ( $-0.05$ ). Ultimately, this suggests that the trend in the behaviour does not vary much, although the absolute values of  $\eta_{ts}$  do.

Alongside the power output, the resulting turbine volumetric expansion ratios should also be considered, and these are reported in Fig. 12(a). The turbine volumetric expansion ratio is defined as the change in density across the whole turbine (*i.e.*,  $\rho_3/\rho_5$ ). It is observed that this is significantly affected by the expander inlet vapour quality, but is less sensitive to the degree of reaction. For example, for  $R = 0.1$ , the turbine volumetric ratio increases from 20 to 250, as  $x_3$  is reduced from 0.9 to 0.1. This increase is the result of introducing more liquid, which has a much higher density than vapour, into the turbine inlet. Alongside the turbine volumetric expansion ratio, it is also interesting to consider the change in density across only the stator (*i.e.*,  $\rho_3/\rho_4$ ), which is reported in Fig. 12(b). Ultimately, these results are similar to Fig. 12(a), with  $x_3$  having a significant effect on the change in density across the stator. However, the stator volumetric expansion ratio is more affected by the degree of reaction, with lower reaction leading to higher changes in density. This is not surprising since a lower degree of reaction corresponds to a larger amount of expansion within the stator. Consequently, considering that the optimal cycles are independent of the degree of reaction (provided  $R < 0.4$ ) and thus have similar turbine volumetric expansion ratios, this means that the volumetric expansion ratios within the rotor will be reduced as the reaction is reduced. For example, for  $x_3 = 0.1$  the turbine volumetric expansion ratios range between 250 and 255 for  $R < 0.4$ . The stator volumetric expansion ratios for  $R = 0.1$  and  $0.4$  are 139 and 77 respectively, whilst the rotor volumetric expansion ratios are 1.8 and 3.3.

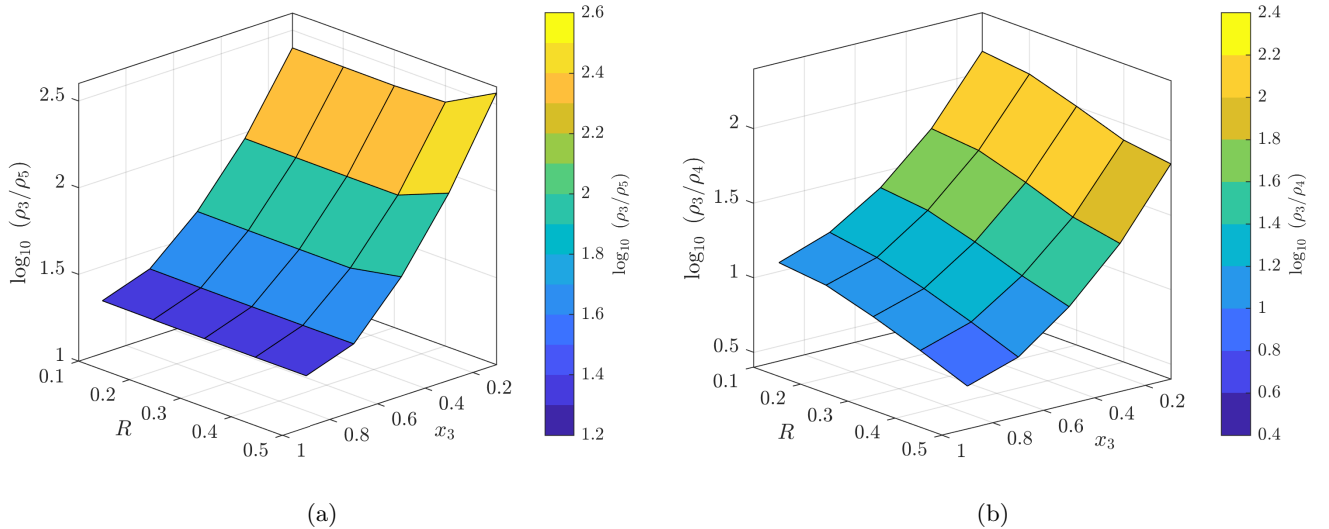


Figure 12: Effect of turbine inlet vapour quality and degree of reaction on: (a) turbine volumetric expansion ratio ( $\rho_3/\rho_5$ ); (b) stator volumetric expansion ratio ( $\rho_3/\rho_4$ ).

Considering the rotor geometry a number of observations are made. Firstly, it is found that the rotational speed for all turbines range between 15,000 and 26,000 rpm, with specific speeds ranging between 0.34 and 0.55, which are in line with expected values for a turbine with a power rating of a few tens of kilowatts. As expected, the higher rotational speeds, and specific speeds, correspond to higher degrees of reaction. The rotor diameters vary

between 123 and 190 mm, and show the opposite trend with diameter reducing as the degree of reaction is increased. The corresponding rotor inlet blade speeds range between 146 and 235 m/s, which are well within the limits for a single-stage radial turbine. Finally, the rotor inlet blade heights are found to range between 3.75 and 7.92 mm.

Regarding the stator design, the resulting rotor-inlet absolute Mach numbers are reported in Fig. 13. Owing to the large expansion ratios, all designs require a converging-diverging stator to deliver the flow to the rotor at the required Mach number, which ranges between 1.56 and 2.04. Moreover, as the degree of reaction is reduced, the required Mach number increases, with the maximum found for  $x_3 = 0.1$  and  $R = 0.1$ . As a rough initial approximation, it is assumed that the stator is constructed from 16 stator vanes. The corresponding stator throat widths, based on the assumption of a homogeneous two-phase fluid at thermal equilibrium, range between 0.93 and 3.80 mm with lower vapour qualities corresponding to smaller throat widths; the minimum value was found for  $x_3 = 0.1$  and  $R = 0.2$ . Thus, reconsidering the analysis relating to Fig. 11, the best design from both the thermodynamic and turbine efficiency point of view, not only leads to a large stator volumetric expansion ratio, but will also be more affected by losses related to supersonic flow, and require an extremely small stator throat width. These results warrant some caution on the validity on the stator loss coefficient (Eq. 9) under these conditions and require further investigation to establish whether such stator designs can be achieved in practice.

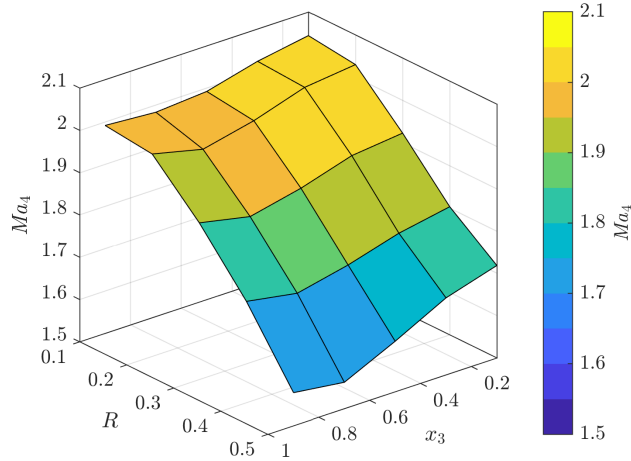


Figure 13: Effect of turbine inlet vapour quality and degree of reaction rotor-inlet absolute Mach number.

Considering the rotor flow conditions, which are not presented for brevity, it is noted that the maximum rotor inlet relative Mach number is at a maximum for  $x_3 = 0.1$  and  $R = 0.1$ , and approaches unity indicating that the relative flow conditions are at the limit of subsonic flow for low reaction; for a higher degree of reaction the relative Mach number reduces to around 0.27 ( $R = 0.5$ ). At the rotor outlet the relative Mach numbers are also below unity although opposite trends are observed with higher reaction leading to relative Mach numbers that approach unity. This indicates that a turbine can be designed with flow conditions that remain subsonic within the rotor.

Overall, an optimal design for the cycle and turbine is obtained at  $x_3 = 0.1$  and  $R = 0.4$ . For the same cycle operating conditions, the cycle analysis suggests that similar performance could be obtained with degrees of reaction as low as 0.1, although the turbine optimisation revealed this will reduce the turbine isentropic efficiency. However, the lower degree of reaction design could facilitate dry rotor-inlet conditions to be obtained across a wider range

of operation conditions and thus widen the operational envelope of the machine. For this reason, alongside the uncertainty in the stator performance, two candidate turbine designs with varying degrees of reaction have been identified. The design parameters for these two turbines are summarised in Tab. 8 and the meridional profiles are reported in Fig. 14. These two turbine designs will be evaluated in more detail in later studies.

Table 8: Design parameters for the two candidate designs selected for further investigation.

$x_3$	$R$	$\psi$	$\phi$	$\eta_{ts}$ [%]	$\dot{W}_t$ [kW]	$N$ [kRPM]	$N_s$	$\alpha_4$ [°]	$\beta_4$ [°]	$\alpha_5$ [°]	$\beta_5$ [°]	$Ma_4$	$Ma_{4'}$	$Ma_{5'}$	$o_{th}$ [mm]
0.1	0.4	1.16	0.17	87.2	20.9	20.6	0.43	80.0	40.4	10.3	-73.9	1.80	0.41	0.93	1.08
0.1	0.1	1.59	0.50	69.8	16.8	16.3	0.35	71.8	51.7	21.2	-41.1	2.04	1.03	0.75	1.18

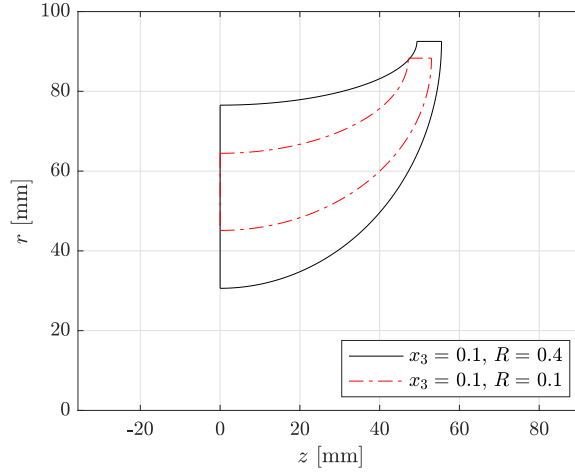


Figure 14: Rotor meridional profiles for the two candidate designs selected for further investigation.

## 5. Conclusions

This paper has for the first time explored the thermodynamic optimisation, working-fluid selection and mean-line turbine design for a two-phase organic Rankine cycle (ORC) operating with organic fluids that facilitate a wet-to-dry expansion process. This architecture allows a radial-inflow turbine to be selected as the expansion machine, potentially facilitating high expander isentropic efficiencies to be obtained, whilst retaining the thermodynamic benefit of two-phase expansion that could improve the power output from waste-heat recovery systems based on ORC technology by up to 30%. Ultimately, this could reduce the cost of these systems, which would aid in the more widespread deployment of ORC technology to recover the significant amount of waste heat that is available at temperatures below 300 °C (approximately 54 PWh globally).

The first outcome of this study is the identification of the most promising fluids and cycle operating conditions that achieve the targeted improvement in power output. For heat-source temperature of 150, 200 and 250 °C thermodynamic cycle optimisation has revealed that the two-phase system can respectively produce up to 28%, 14% and 3.3% more power than equivalent optimal baseline ORC systems operating with single-phase expansion. Moreover, a multi-objective optimisation considering the trade-off between thermodynamic performance and heat-exchanger size has revealed that two-phase cycles could have benefits over single-phase cycles across a broader range

of applications than just applications where the objective is to maximise power. Optimal fluids are found to be those with high molecular complexity, including siloxanes (MM and MDM) and Novec649. However, consideration should be given to the resulting pressure ratio and condensation pressure, which influence the cycle component design.

The second outcome of this study is the extension of existing mean-line design methods for single-phase ORC turbines to radial-inflow turbines operating with two-phase inlet conditions, and the generation of candidate turbine designs with an indicated high isentropic efficiency that will be studied further in following studies. Existing rotor loss models are deployed for evaluating the rotor performance, whilst given that this is the first study of its kind and no experimental data or numerical results are available for two-phase ORC stator vanes, a loss correlation has been developed based on numerical 3D CFD simulations completed under the assumption of a two-phase homogeneous fluid under thermal equilibrium. Further investigations are required to investigate whether this assumption is valid. Results from a parametric mean-line turbine optimisation study reveal that maximum thermodynamic performance and maximum turbine isentropic efficiency can be achieved at low turbine inlet vapour qualities and high degrees of reaction, with lower reaction leading to lower turbine efficiencies. For the case of MM for the 200 °C heat source, the optimal conditions correlate to a turbine vapour inlet quality of 0.1 and degree of reaction of 0.4. Moreover, it is observed that feasible rotor geometries can be obtained, and conditions with the rotor are expected to remain subsonic. On the other hand, supersonic stator vanes are required that can deliver the flow to the rotor inlet at Mach numbers in the range of 1.5 to 2.1, with throat widths as low as 0.9 mm. However, the CFD simulations provide the first indication that a full transition from saturated two-phase conditions to superheated vapour can be achieved within the stator. In summary, these results provide the first positive indication that the goal of designing a two-phase ORC system based on a radial-inflow turbine with dry conditions at the rotor inlet can be successfully realised, and the target of a 30% improvement in power output achieved.

## Acknowledgements

This project was supported by the Royal Academy of Engineering under the Research Fellowship scheme (2019–2024). Award number: RF\201819\18\23.

## References

- [1] C. Forman, I. K. Muritala, R. Pardemann, B. Meyer, Estimating the global waste heat potential, *Renewable and Sustainable Energy Reviews* 57 (2016) 1568–1579. doi:10.1016/j.rser.2015.12.192.
- [2] G. Bianchi, G. P. Panayiotou, L. Aresti, S. A. Kalogirou, G. A. Florides, K. Tsamos, S. A. Tassou, P. Christodoulides, Estimating the waste heat recovery in the European Union industry, *Energy, Ecology and Environment* 4 (5) (2019) 211–221. doi:10.1007/s40974-019-00132-7.
- [3] I. K. Smith, Development of the trilateral flash cycle system: Part 1: Fundamental considerations, *Proceedings of the Institution of Mechanical Engineers, Part A: Journal of Power and Energy* 207 (3) (1993) 179–194. doi:10.1243/pime\_proc\_1993\_207\_032\_02.

- [4] J. Fischer, Comparison of trilateral cycles and organic Rankine cycles, *Energy* 36 (10) (2011) 6208–6219. doi:10.1016/j.energy.2011.07.041.
- [5] N. A. Lai, J. Fischer, Efficiencies of power flash cycles, *Energy* 44 (1) (2012) 1017–1027. doi:10.1016/j.energy.2012.04.046.
- [6] I. K. Smith, N. Stosic, C. A. Aldis, Development of the trilateral flash cycle system: Part 3: The design of high-efficiency two-phase screw expanders, *Proceedings of the Institution of Mechanical Engineers, Part A: Journal of Power and Energy* 210 (1) (1996) 75–93. doi:10.1243/pime\_proc\_1996\_210\_010\_02.
- [7] H. Öhman, P. Lundqvist, Experimental investigation of a Lysholm turbine operating with superheated, saturated and 2-phase inlet conditions, *Applied Thermal Engineering* 50 (1) (2013) 1211–1218. doi:10.1016/j.applthermaleng.2012.08.035.
- [8] G. Bianchi, R. McGinty, D. Oliver, D. Brightman, O. Zaher, S. A. Tassou, J. Miller, H. Jouhara, Development and analysis of a packaged trilateral flash cycle system for low grade heat to power conversion applications, *Thermal Science and Engineering Progress* 4 (2017) 113–121. doi:10.1016/j.tsep.2017.09.009.
- [9] Electratherm, <https://electratherm.com/products/> [Last accessed: 17/11/2020].
- [10] Heliex Power, <https://www.heliexpower.com/> [Last accessed: 17/11/2020].
- [11] M. G. Read, I. K. Smith, N. Stosic, Optimisation of power generation cycles using saturated liquid expansion to maximise heat recovery, *P I Mech Eng E-J Pro* 23 (1) (2017) 57–69. doi:10.1177/0954408916679202.
- [12] O. Dumont, R. Dickes, V. Lemort, Experimental investigation of four volumetric expanders, *Energy Procedia* 129 (2017) 859–866. doi:10.1016/j.egypro.2017.09.206.
- [13] B. Staniša, V. Ivušić, Erosion behaviour and mechanisms for steam turbine rotor blades, *Wear* 186-187 (1995) 395–400. doi:10.1016/0043-1648(95)07136-9.
- [14] L. G. Hays, Two-phase turbines for compressor energy recovery, in: *International Compressor Engineering Conference*, Purdue, USA, 1996, pp. 657–662.
- [15] P. Welch, P. Boyle, New turbines to enable efficient geothermal power plants, in: *Geothermal Resources Council Transactions*, Vol. 33, 2009, pp. 765–772.
- [16] S. Rane, L. He, Two-phase flow analysis and design of geothermal energy turbine, *IOP Conference Series: Materials Science and Engineering* 604 (2019) 012043. doi:10.1088/1757-899x/604/1/012043.
- [17] H. Li, S. Rane, Z. Yu, G. Yu, An inverse mean-line design method for optimizing radial outflow two-phase turbines in geothermal systems, *Renewable Energy* 168 (2021) 463–490. doi:10.1016/j.renene.2020.12.079.
- [18] A. Date, A. Khaghani, J. Andrews, A. Akbarzadeh, Performance of a rotating two-phase turbine for combined power generation and desalination, *Applied Thermal Engineering* 76 (2015) 9–17. doi:10.1016/j.applthermaleng.2014.08.074.

- [19] M. Ahmadi, S. Vahaji, M. Arbab Iqbal, A. Date, A. Akbarzadeh, Experimental study of converging-diverging nozzle to generate power by trilateral flash cycle (TFC), *Applied Thermal Engineering* 147 (2019) 675–683. doi:10.1016/j.applthermaleng.2018.10.116.
- [20] S. Rane, L. He, Numerical analysis of a novel two-phase turbine using thermal non-equilibrium, homogeneous nucleation phase change, *Thermal Science and Engineering Progress* 22 (December 2020). doi:10.1016/j.tsep.2020.100827.
- [21] D. G. Elliott, Theory and tests of two-phase turbines, Tech. rep., Jet Propulsion Laboratory, California Institute of Technology, Pasadena, California (1982).
- [22] E. Lemmon, M. Huber, M. McLinden, NIST standard reference database 23: Reference fluid thermodynamic and transport properties-REFPROP (2013).
- [23] M. A. Chatzopoulou, S. Lecompte, M. D. Paepe, C. N. Markides, Off-design optimisation of organic Rankine cycle (ORC) engines with different heat exchangers and volumetric expanders in waste heat recovery applications, *Applied Energy* 253 (January) (2019) 113442. doi:10.1016/j.apenergy.2019.113442.
- [24] T. W. Lim, Y. S. Choi, Thermal design and performance evaluation of a shell-and-tube heat exchanger using LNG cold energy in LNG fuelled ship, *Applied Thermal Engineering* 171 (January) (2020) 115120. doi:10.1016/j.applthermaleng.2020.115120.
- [25] The Matworks Inc., Global Optimization Toolbox (2017).
- [26] L. D. Lio, G. Manente, A. Lazzaretto, A mean-line model to predict the design efficiency of radial inflow turbines in organic Rankine cycle (ORC) systems, *Applied Energy* 205 (July) (2017) 187–209. doi:10.1016/j.apenergy.2017.07.120.
- [27] S. Bahamonde, M. Pini, C. De Servi, A. Rubino, P. Colonna, Method for the preliminary fluid dynamic design of high-temperature mini-organic Rankine cycle turbines, *Journal of Engineering for Gas Turbines and Power* 139 (8) (2017) 082606. doi:10.1115/1.4035841.
- [28] A. Meroni, M. Robertson, R. Martinez-Botas, F. Haglind, A methodology for the preliminary design and performance prediction of high-pressure ratio radial-inflow turbines, *Energy* 164 (2018) 1062–1078. doi:10.1016/j.energy.2018.09.045.
- [29] K. Rahbar, S. Mahmoud, R. K. Al-Dadah, N. Moazami, Parametric analysis and optimization of a small-scale radial turbine for organic Rankine cycle, *Energy* 83 (1) (2015) 696–711. doi:10.1016/j.energy.2015.02.079.
- [30] C. Rodgers, Mainline performance prediction for radial inflow turbines, in: C. Sieverding (Ed.), *Lecture Series on Small High Pressure Ratio Turbines*, Von Karman Institute for Fluid Dynamics, 1987.
- [31] P. Colonna, N. R. Nannan, A. Guardone, E. W. Lemmon, Multiparameter equations of state for selected siloxanes, *Fluid Phase Equilibria* 244 (2) (2006) 193–211. doi:10.1016/j.fluid.2006.04.015.

- [32] J. Harinck, D. Pasquale, R. Pecnik, J. V. Buijtenen, P. Colonna, Performance improvement of a radial organic Rankine cycle turbine by means of automated computational fluid dynamic design, Proceedings of the Institution of Mechanical Engineers, Part A: Journal of Power and Energy 227 (6) (2013) 637–645.
- [33] C. M. De Servi, M. Burigana, M. Pini, P. Colonna, Design method and performance prediction for radial-inflow turbines of high-temperature mini-organic Rankine cycle power systems, Journal of Engineering for Gas Turbines and Power 141 (9) (2019) 091021. doi:10.1115/1.4043973.
- [34] F. J. Durá Galiana, A. P. Wheeler, J. Ong, A study of trailing-edge losses in organic Rankine cycle turbines, Journal of Turbomachinery 138 (12) (2016) 121003. doi:10.1115/1.4033473.
- [35] G. J. Otero R, S. H. Smit, R. Pecnik, Three-dimensional unsteady stator-rotor interactions in high-expansion organic Rankine cycle turbines, Energy 217 (2021) 119339. doi:10.1016/j.energy.2020.119339.
- [36] M. White, The design and analysis of radial inflow turbines implemented within low temperature organic Rankine cycles, Phd, City, University of London (2015).
- [37] N. Baines, Part 3: Radial Turbine Design, in: Axial and Radial Turbines, 2003, Ch. 7-9.
- [38] S. L. Dixon, Fluid Mechanics and Thermodynamics of Turbomachinery, 5th Edition, Butterworth-Heinemann, 2005.
- [39] C. E. Brennen, Fundamentals of multiphase flow, Cambridge University Press, 2005. doi:10.1017/CB09780511807169.

## Appendix A. Turbine design methodology

### Appendix A.1. Mean-line design methodology

For a defined thermodynamic specification obtained from the the cycle analysis, a specified degree of reaction and set of turbine design variables, the procedure that is applied to optimise the mean-line design of the turbine is outlined in Fig. A.15.

The rotor velocity triangles are computed by first calculating the stage enthalpy drop  $\Delta h_0$  from the thermodynamic conditions and assumed turbine isentropic efficiency. The stage enthalpy drop can then be related to the change in angular momentum across the rotor through Euler’s turbomachinery equation:

$$\frac{\dot{W}}{\dot{m}} = \Delta h_0 = u_4 c_{\theta 4} - u_5 c_{\theta 5} , \quad (\text{A.1})$$

where  $u$  and  $c_\theta$  indicate the blade speed and absolute tangential velocities respectively, as depicted in Fig. 8. The meridional velocities at inlet and outlet,  $c_{m4}$  and  $c_{m5}$ , alongside  $u_4$  and  $u_5$ , follow directly from the specified design variables ( $\psi$ ,  $\phi$ ,  $\xi$ ,  $\varepsilon$ ). To determine the rotor-inlet tangential velocity  $c_{\theta 4}$  that corresponds to the desired degree of reaction, the following quadratic equation is solved:

$$a_1 c_{\theta 4}^2 + a_2 c_{\theta 4} + a_3 = 0 , \quad (\text{A.2})$$

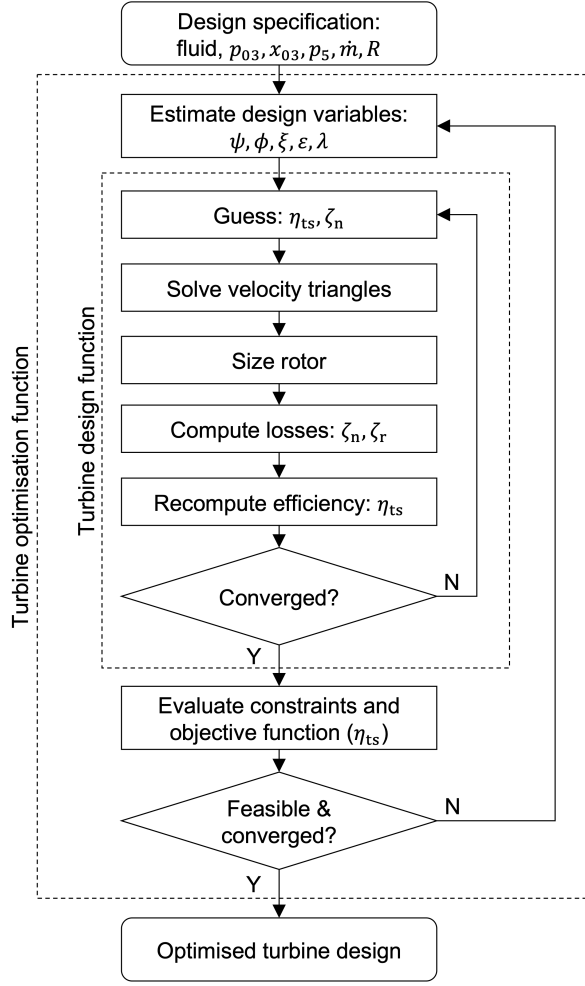


Figure A.15: Design optimisation procedure for the two-phase turbine.

where,

$$a_1 = \frac{1}{\varepsilon^2} - \frac{1}{1-R};$$

$$a_2 = -\frac{2\sqrt{\psi\Delta h_0}}{\varepsilon^2};$$

$$a_3 = \Delta h_0 \left[ \frac{\psi}{\varepsilon^2} - \frac{\phi^2}{\psi(1-R)} + 2 + \frac{(\phi\xi)^2}{\psi} \right].$$

which is derived by combining Eq. A.1 with the definitions of the design variables and considering the geometrical relations depicted in Fig. 8. The rotor-outlet tangential velocity  $c_{\theta 5}$  follows from Euler's turbine equation after which the remaining velocities can be calculated.

Once the velocities are known, the total and static conditions at the rotor inlet and outlet follow based on the current values for  $\eta_n$  and  $\eta_{ts}$ . The rotor dimensions are then obtained by sizing the rotor inlet and outlet to pass the

desired mass-flow rate:

$$A_4 = \frac{\dot{m}}{\rho_4 c_{m4}} = \pi d_4 b_4 (1 - BK_4); \quad (\text{A.3})$$

$$A_5 = \frac{\dot{m}}{\rho_5 c_{m5}} = \left(\frac{\pi}{4}\right) (d_{5s}^2 - d_{5h}^2) (1 - BK_5), \quad (\text{A.4})$$

where  $BK$  are blockage factors. These are calculated according to the method detailed in Ref. [36].

Following rotor sizing, the stator and rotor loss coefficients are computed, which are defined respectively as:

$$\zeta_n = \frac{h_4 - h_{4s}}{\frac{1}{2}c_4^2}; \quad (\text{A.5})$$

$$\zeta_r = \frac{h_5 - h_{5s}}{\frac{1}{2}w_5^2}, \quad (\text{A.6})$$

where  $h_{4s}$  and  $h_{5s}$  are the enthalpies following an isentropic expansion within the stator and rotor respectively. Once  $\zeta_n$  and  $\zeta_r$  are known, the next guess for the turbine isentropic efficiency is estimated from:

$$\eta_{ts} = \left( 1 + \frac{c_5^2 + \zeta_r w_5^2 + \zeta_n \left(\frac{T_5}{T_4}\right) c_4^2}{2\Delta h_0} \right)^{-1}. \quad (\text{A.7})$$

As noted in the main body, the rotor loss coefficient is computed using loss models for the passage, trailing-edge, post-expansion, clearance and disc friction losses that are detailed in Ref. [28], with the omission of incidence loss since the current study deals only with design-point performance. The stator loss coefficient is estimated using the correlation derived from the CFD investigations (Eq. 9).

#### *Appendix A.2. Mean-line design verification*

A qualitative verification of the turbine design model for two-phase operation, integrating the rotor loss models with Eq. 9, is reported in Fig. A.16. Within this figure, the isentropic efficiency is reported for a representative turbine specification across a range of loading and flow coefficients. The behaviour observed is consistent with similar plots reported within the literature [37, 38]. It should however be noted that in the current work the region of high efficiency is found at higher values of  $\psi$  and lower values of  $\phi$ , which could be attributed to the current work allowing non-zero inlet blade angles and thus positive relative flow angles. It is also noted that efficiencies in the region of 88% are likely to be difficult to achieve in practice, and this over estimation could be due to Eq. 9 which requires further investigation. But nonetheless, the results in Fig. A.16 are considered to provide a reasonable initial verification that the model is able to adequately capture the relative variation in  $\eta_{ts}$  with key turbine design parameters.

#### *Appendix A.3. Stator design methodology*

To investigate the loss coefficient for a two-phase stator a design methodology has been developed to generate a number of candidate stator designs that have been evaluated using computational-fluid dynamic simulations. A schematic of the proposed stator geometry, alongside the defined notation, is provided in Fig. A.17.

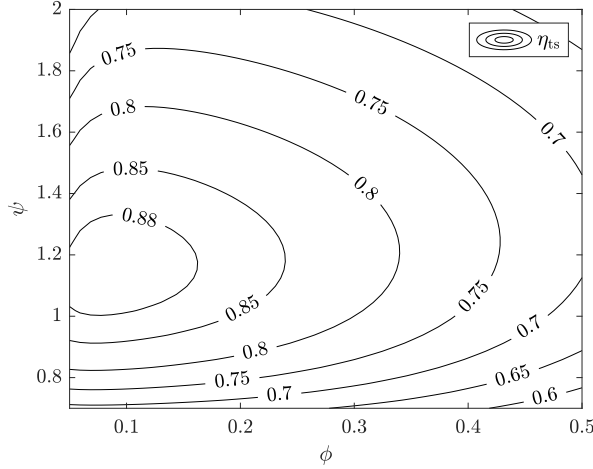


Figure A.16: Contour map of turbine isentropic efficiency  $\eta_{ts}$  as a function of loading coefficient  $\psi$  and flow coefficient  $\phi$ . Generated for MM using the following inputs:  $p_3 = 675$  kPa,  $x_3 = 0.1$ ,  $R = 0.4$ ,  $p_3/p_5 = 40$ ,  $\dot{m} = 0.45$  kg/s,  $\xi = 1$ ,  $\varepsilon = 0.6$ ,  $\lambda = 0.4$ .

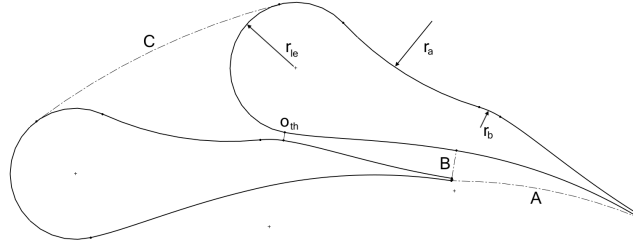


Figure A.17: Schematic and notation used to describe the two-phase stator design.

For a given turbine specification, and a suitable estimate for the stator loss coefficient, the thermodynamic conditions at the rotor inlet are known. From this, the stator outlet radius  $r_A$  is determined based on an input interspace radius ratio  $r_A/r_4$ , and the conditions at the stator outlet are computed by applying the conservation of mass, energy and momentum across the rotor-stator interspace assuming an isentropic expansion. Moreover, for a specified number of stator blades  $Z_n$ , a similar application of the conservation of mass, energy and momentum between the stator outlet (station A) and the outlet of the converging-diverging nozzle (station B) yields the static pressure  $p_B$  and flow angle  $\alpha_B$ .

The stator vane chord length  $C_n$ , which corresponds to the length of the converging-diverging nozzle, is obtained from a specified value for the chord to throat ratio  $C_n/o_{th}$ . Assuming the nozzle takes the form of a planar nozzle with a passage width that is equal to the rotor-inlet blade height, the stator throat size is determined from:

$$o_{th} = \frac{\dot{m}}{\rho^* a^* Z_n b_4}, \quad (\text{A.8})$$

where  $\rho^*$  and  $a^*$  are the density and speed of sound at the throat. Assuming homogeneous, thermal-equilibrium conditions the speed of sound for a two-phase fluid can be determined using the method described in Ref. [39].

A Bezier curve is used to construct the pressure profile within the converging diverging nozzle, with the conditions  $dp/dx|_{x=0} = dp/dx|_{x=C_n} = 0$ ,  $p(x=0) = p_C$ ,  $p(x=C_n) = p_B$  and  $p(x=C_n/2) = (p_B + p_C)/2$ , where  $x$  refers to

the distance along the nozzle axis and  $p_C$  is calculated assuming a prescribed inlet velocity to the stator. The nozzle profile is then constructed assuming one-dimensional isentropic expansion from the turbine inlet conditions.

Once the nozzle is defined it is positioned at the stator outlet radius and rotated according to the required stator outlet flow angle. Then a number of manual geometrical modifications are required to complete the stator design: (i) the nozzle profile upstream of the throat is removed and replaced with a leading edge circular arc with a radius that conserves the defined stator chord length,  $r_{le}$ ; (ii) two additional circular arcs are used to construct the remaining part of the upper side of the blade upstream of the throat,  $r_a$  and  $r_b$ ; and (iii) the bladed region downstream of the nozzle is constructed in order to conserve the flow angle between stations A and B.

Ultimately, the process outlined here is not expected to lead to an optimised design, but instead has been developed to allow the rapid generation of preliminary stator designs that can be assessed for the purposes of this study. The topic of stator design optimisation for two-phase expansion is left for a later work, which could also include a consideration of partial-admission or non-planar stator designs with a varying passage height to mitigate potential issues relating to the large expansion ratio across the stator vane.

## Nomenclature

### Abbreviations

ORC organic Rankine cycle

### Symbols

$\alpha$	absolute flow angle, °
$\beta$	relative flow angle, °
$\Delta T_{\log}$	log-mean temperature difference, K
$\delta_{cl}$	clearance gap, mm
$\dot{m}$	mass-flow rate, kg/s
$\dot{W}$	power, J/s
$\eta$	isentropic efficiency
$\lambda$	rotor hub/shroud diameter ratio
$BK$	blockage factor
$Ma$	Mach number
$\mu$	dynamic viscosity, Pa s
$\phi$	flow coefficient
$\psi$	blade loading coefficient
$\rho$	density, kg/m <sup>3</sup>
$\tau$	heat-capacity rate ratio
$\theta$	non-dimensional heat-source temperature drop
$\varepsilon$	rotor outlet/inlet diameter ratio
$\xi$	meridional velocity ratio
$\zeta$	loss coefficient
$A$	heat-transfer area, m <sup>2</sup>
$b$	blade height, m
$c$	absolute velocity, m/s
$c_p$	specific-heat capacity at constant pressure, J/(kg K)
$d$	diameter, m
$h$	specific enthalpy, J/kg
$L$	axial length, m
$N$	rotational speed, rpm
$N_s$	specific speed
$o_{th}$	throat width, mm
$p$	pressure, Pa
$p_r$	reduced evaporation pressure

$PP$	pinch point, K
$R$	degree of reaction
$s$	specific entropy, J/(kg K)
$T$	temperature, K
$U$	overall heat-transfer coefficient, W/(m <sup>2</sup> K)
$u$	blade velocity, m/s
$w$	relative velocity, m/s
$x$	expander inlet parameter
$Z$	number of blades

### Subscripts

'	saturated conditions, relative
*	throat conditions
$\theta$	tangential velocity component
0	stagnation conditions
1-5	cycle and turbine state points
c	heat sink
cr	critical point
h	heat source, hub
i	inlet
m	meridional velocity component
min	minium
n	net, nozzle
o	outlet
p	pump
r	rotor
s	conditions after isentropic expansion, shroud
t	turbine
ts	total-to-static

## List of Figures

1	Comparison between an ORC operating with single-phase (left) and two-phase (right) expansion from an open heat source. . . . .	3
2	Saturation curves for the most promising fluid candidates viewed in the $T$ - $s$ plane. . . . .	5
3	Notation used to describe the ORC system operating with two-phase expansion. . . . .	6
4	Results from the single-objective optimisation for the two-phase cycles with $T_{hi} = 200$ °C; (a) optimal power output and expander inlet vapour quality; (b) optimal pressure ratio and condensation pressures; (c) heat-exchanger requirements; (d) optimal MDM two-phase cycle; (e) optimal MM two-phase cycle; (f) optimal base-line non-recuperated single-phase cycle with Novec649. In (a)-(c) the number in brackets after the working fluid refers to degree of reaction. . . . .	10
5	Sensitivity of the single-objective optimisation results to the isentropic efficiencies for the pump $\eta_p$ , turbine $\eta_t$ and stator $\eta_n$ . . . . .	12
6	Results from the multi-objective optimisation for $T_{hi} = 200$ °C; the top plot compares the Pareto fronts obtained for two-phase cycles operating with MDM and MM at different degrees of reaction to non-recuperated (non-recup.) and recuperated (recup.) single-phase cycles; the bottom reports the variation in the expander inlet parameter $x_3$ across the Pareto fronts. . . . .	12
7	Representative optimal two-phase cycles shown on a $T$ - $s$ diagram taken from the Pareto fronts obtained from the multi-objective optimisation. The top row corresponds to MDM with $R = 0.1$ , and the bottom row corresponds to MM with $R = 0.1$ . . . . .	13
8	Notation used to define the radial turbine design. . . . .	15
9	Contours of mid-span mass fraction, Mach number and static entropy for Case 1 ( $p_{03} = 500$ kPa; $q_{03} = 0.3$ ; $b_4 = 1.496$ mm). . . . .	20
10	Relationship between passage height $b_4$ and stator loss coefficient $\zeta_n$ obtained using CFD for the four stator designs. . . . .	21
11	Effect of turbine inlet vapour quality and degree of reaction on the performance of the two-phase system operating with MM: (a) power output predicted by thermodynamic cycle where at each point the optimal cycle conditions are obtained using the cycle model reported in Section 3 assuming a fixed turbine efficiency; (b) optimal total-to-static isentropic efficiency obtained from the mean-line turbine design optimisation. Note that for visualisation purposes the axes in (b) have been flipped. . . . .	22
12	Effect of turbine inlet vapour quality and degree of reaction on: (a) turbine volumetric expansion ratio ( $\rho_3/\rho_5$ ); (b) stator volumetric expansion ratio ( $\rho_3/\rho_4$ ). . . . .	23
13	Effect of turbine inlet vapour quality and degree of reaction rotor-inlet absolute Mach number. . . . .	24
14	Rotor meridional profiles for the two candidate designs selected for further investigation. . . . .	25
A.15	Design optimisation procedure for the two-phase turbine. . . . .	30
A.16	Contour map of turbine isentropic efficiency $\eta_{ts}$ as a function of loading coefficient $\psi$ and flow coefficient $\phi$ . Generated for MM using the following inputs: $p_3 = 675$ kPa, $x_3 = 0.1$ , $R = 0.4$ , $p_3/p_5 = 40$ , $\dot{m} = 0.45$ kg/s, $\xi = 1$ , $\varepsilon = 0.6$ , $\lambda = 0.4$ . . . . .	32

A.17 Schematic and notation used to describe the two-phase stator design. . . . . 32

**List of Tables**

1	Working-fluid candidates. . . . .	5
2	Defined heat-source and heat-sink conditions. . . . .	9
3	Initial assumptions for the cycle optimisation study. . . . .	9
4	Comparison of non-recuperated single- and two-phase cycles for a range of heat-source and heat-sink conditions. The percentages reported in brackets indicate a negative impact. . . . .	14
5	Fixed and variable design inputs and constraints for the design optimisation of the two-phase radial-inflow turbine. . . . .	17
6	Validation of the rotor mean-line design model against Ref. [29]. . . . .	18
7	Stator design parameters. . . . .	19
8	Design parameters for the two candidate designs selected for further investigation. . . . .	25